Title

Synovial fibroblasts contribute to the genetic risk of rheumatoid arthritis through the synergistic action of cytokines

Authors

Haruka Tsuchiya[1,9], Mineto Ota[1,2,3,9,*], Shuji Sumitomo[1], Kazuyoshi Ishigaki[4], Akari Suzuki[3], Toyonori Sakata[5], Yumi Tsuchida[1], Hiroshi Inui[8], Jun Hirose[8], Yuta Kochi[3,6], Yuho Kadono[7], Katsuhiko Shirahige[5], Sakae Tanaka[8], Kazuhiko Yamamoto[3], Keishi Fujio[1,10,*]

Affiliations

[1]Department of Allergy and Rheumatology, Graduate School of Medicine, The University of Tokyo, Tokyo, 113-0033, Japan

[2]Department of Functional Genomics and Immunological Diseases, Graduate School of Medicine, The University of Tokyo, Tokyo, 113-0033, Japan

[3]Laboratory for Autoimmune Diseases, RIKEN Center for Integrative Medical Sciences, Yokohama, 230-0045, Japan

[4]Divisions of Genetics and Rheumatology, Department of Medicine, Brigham and Women's Hospital, Harvard Medical School, Boston, MA 02115, USA

[5]Laboratory of Genome Structure and Function, Institute for Quantitative Biosciences, The University of Tokyo, Tokyo, 113-0032, Japan

[6]Department of Genomic Function and Diversity, Medical Research Institute, Tokyo Medical and Dental University, Tokyo, 113-8510, Japan

[7]Department of Orthopaedic Surgery, Saitama Medical University, Saitama, 350-0495, Japan.

[8]Department of Orthopaedic Surgery, Graduate School of Medicine, The University of Tokyo, Tokyo, 113-0033, Japan

[9]These authors contributed equally

[10]Lead contact: kfujio-tky@umin.ac.jp

*Correspondence: K.F., kfujio-tky@umin.ac.jp; M.O., mioota-tky@umin.ac.jp

Summary

In rheumatoid arthritis (RA), synovial fibroblasts (SFs) produce pathogenic molecules in the inflamed synovium. Despite their potential importance, comprehensive understanding of SFs under inflammatory conditions remains elusive. Here, to elucidate the actions of SFs and their contributions to RA pathogenesis, we stimulated SFs with 8 proinflammatory cytokines and analyzed the outcome using genomic, epigenomic and transcriptomic approaches. We observed stimulated transcription of pathogenic molecules by SFs exposed to synergistically acting cytokines. Some RA risk loci were associated with the expression of certain specific genes. We also observed epigenomic remodeling in activated SFs. Moreover, RA risk loci were enriched in clusters of enhancers (super-enhancers) exposed to synergistic proinflammatory cytokines. Our results shed light on the importance of activated SFs in RA pathogenesis. They also suggest possible treatment strategies targeting epigenomic alterations in SFs by inhibition of candidate modulators including MTF1 and RUNX1.

Key words

Rheumatoid arthritis, synovial fibroblasts, cytokine synergy, RNA sequencing, ChIP sequencing, Hi-C, expression quantitative trait locus analysis, super enhancers, MTF1, RUNX1

Introduction

Rheumatoid arthritis (RA) is an autoimmune disease that affects ~1% of the population worldwide and causes persistent synovial inflammation leading to disabling joint destruction. In the pathogenesis of RA, the activities of a variety of dysregulated molecules in immune cells (e.g., T cells, B cells, monocytes) and mesenchymal cells are orchestrated by genetic and environmental factors (Chen et al., 2019; Smolen et al., 2018). Twin studies have estimated that the heritability of RA is as high as 60% (Aho et al., 1986; Silman et al., 1993), and more than 100 RA susceptibility loci have been identified in genome-wide association studies (GWAS) (Okada et al., 2019; Okada et al., 2014). Recent genetic studies of autoimmune diseases have reported that the majority (> 90%) of these risk variants are located in non-coding regions and regulate the expression levels of a number of genes in a cell type-specific manner (Farh et al., 2015), partly in an environment-specific fashion (Fairfax et al., 2014). An integrated understanding of the risk variants' contribution to gene regulatory networks is crucial to determine the responsible molecules and cell types in RA pathogenesis.

Synovial fibroblasts (SFs) are the most abundant resident mesenchymal cells of the hyperplastic synovium. They are major local effectors in the initiation and perpetuation of destructive joint inflammation through their production of a variety of immunomodulators, adhesion molecules and matrix-degrading enzymes (Chen et al., 2019; Smolen et al., 2018). For example, SFs are a leading source of IL-6, a central hub in the synovial cytokine network, and its receptor antagonist has shown efficacy for patients with RA (Kang et al., 2019). Previous studies have addressed the transcriptomic or epigenomic basis of RASFs (de la Rica et al., 2013; Nakano et al., 2013; Whitaker et al., 2013). However a comprehensive picture of SFs' contribution to the pathogenesis of RA has largely remained elusive, perhaps due to their complex features that change in response to the proinflammatory milieu (Frank-Bertoncelj et al., 2017; Ospelt et al., 2017; Slowikowski et al., 2018). To date, a number of cytokines that induce the inflammatory behavior of SFs have been reported (e.g., IFN-γ and IL-17 from T cells and TNF-α, IL-1β, IFN-α, IL-18 and TGF-β1 from monocytes) (Leech and Morand, 2013; Takayanagi, 2007). These cytokines activate various signaling pathways (e.g., nuclear factor-kappa B (NF-κB) signaling, Janus kinase (JAK) signaling) *in vitro* that lead to the production of pathogenic molecules from SFs. To make matters more complicated, in the setting of the inflamed synovium, SFs are expected to be exposed to a more complex proinflammatory environment. Data show that some cytokine combinations (e.g., TNF-α and IL-17) (Katz et al., 2001) synergistically enhance the expression of cytokines and chemokines (e.g., IL-1, IL-6 and IL-8). Those findings emphasize the need to analyze the mechanisms underlying the accelerated

inflammatory behavior of SFs in the presence of multiple synergistic factors.

Current treatment strategies that target proinflammatory cytokines (e.g., TNF-α, IL-6), cell surface proteins of immune cells (e.g., CD20, CD80/86) or signaling molecules (e.g., JAK-STAT pathway) have brought a paradigm shift in RA treatment. However, achieving sustained remission with such agents is still challenging, and serious adverse events (e.g., infections, malignancy) due to systemic immune suppression are clinical concerns (van Vollenhoven, 2019). Following the success achieved with blinatumomab (anti-CD19/anti-CD3 antibody) for B cell hematologic malignancies (Kantarjian et al., 2017), the concept of combination therapies (anti-TNF-α and anti-IL-1β or anti-IL-17) or bispecific antibodies (anti-TNF-α/IL-17) were tried in RA patients. Contrary to expectations, they have not achieved success due to the lack of benefits and systemic side effects, including neutropenia (Baker and Isaacs, 2018; Genovese et al., 2004). These findings imply that additional synergistic factors might play critical roles in the progression of synovitis. By elucidating those mechanisms in SFs, safer and more efficient therapeutic strategies might be found to combat the major local effectors in inflamed joints.

Here, we used integrative methods to analyze genomic, transcriptomic and epigenomic features of RASFs in the presence of various proinflammatory cytokines that have been detected in RA joints (Arend and Dayer, 1990; Kokebie et al., 2011). To our knowledge, this study is the first to conduct cis-expression quantitative trait locus (cis-eQTL) analysis of SFs. In this fashion, we demonstrate that SFs exposed to synergistic cytokines show distinct transcriptomic features characterized by elevated expression of pathogenic molecules (i.e., cytokines, chemokines and transcription factors). We also show epigenomic remodeling of SFs under stimulation, and that RA risk loci are enriched in clusters of enhancers (super-enhancers) under the influence of multiple synergistic proinflammatory factors. To achieve this pathogenic epigenomic rearrangement, several transcription factors including MTF1 and RUNX1 may be crucial, suggesting that they might be future targets for RA therapy.

Results

Cytokine mixture induced a distinctive transcriptome signature in SFs.

We stimulated SFs from RA and osteoarthritis (OA) patients (n=30 each) with 8 different cytokines (IFN-α, IFN-γ, TNF-α, IL-1β, IL-6/sIL-6R, IL-17, TGF-β1, IL-18) or a combination of all 8 (8-mix). We also fractionated peripheral blood mononuclear cells (PBMCs) from the same patients into five major immune cell subsets ($CD4^+$ T cells, $CD8^+$ T cells, B cells, NK cells, monocytes), which were not treated with the cytokines (Figure 1).

Next, we quantified mRNA expression by RNA sequencing and compared transcriptome

signatures of SFs between the 10 conditions (i.e., non-stimulated, IFN-α, IFN-γ, TNF-α, IL-1β, IL-6/sIL-6R, IL-17, TGF-β1, IL-18 or 8-mix) and the diseases (i.e., RA, OA). Principal component analysis (PCA) of gene expression levels showed that the 8-mix condition induced a distinct transcriptome signature compared with the other stimulatory conditions, corresponding to the first component (PC1 in Figure 2A, Figure 2B). For instance, the markedly high expression of *IL6*, which codes a pivotal cytokine in RA pathogenesis with a diverse repertoire of functions (e.g., osteoclast differentiation) (Garbers et al., 2018), was achieved by the 8-mix stimulation (Primary component loading on PC1 = -0.76, PC2 = 0.26. Figure 2C). Other genes coding cytokines that are associated with RA (e.g., *MMP3*, *CSF2*) were also significantly upregulated when stimulated by the 8-mix combination (Figure 2C). On the other hand, RASFs showed different transcriptome signatures from OASFs under non-stimulatory or stimulatory conditions, corresponding largely to the second component (PC2 in Figure 2A, Figure 2B). Stimulation by individual cytokines induced unique transcriptomic signatures in SFs (Figure 2A, Figure 2B).

Recently, Fan Zhang and colleagues performed single-cell RNA sequencing analysis of RA and OA synovial cells and reported that SFs could be clustered into 4 fractions (Zhang et al., 2019). To elucidate the association between transcriptional changes of SFs under cytokine stimulation and those 4 fractions, we utilized the gene sets that Fan Zhang *et al.* reported were characteristic of each of the fractions. We then scored our samples with these signatures (Hanzelmann et al., 2013) (STAR Method and Figure S1). Interestingly, the signature score of fraction 4, which was the population abundant in the lining of OA synovium in a previous report (Zhang et al., 2019), was higher in OASFs irrespective of the stimulatory conditions. In contrast, the score of fraction 2, which was a major *IL6* producer and abundant in the sublining of the RA synovium, was not different between RA and OA in non-stimulatory conditions, but they were strongly upregulated under IFN-γ, IFN-α, IL-6 or 8-mix stimulation. Accordingly, we surmised that certain SF populations were quantitatively stable among disease conditions, and some are inducible under cytokine stimulation.

Stimulatory conditions specific to the function of RA genetic risk loci

We next performed cis-eQTL analysis to evaluate how transcription was affected in stimulated SFs and PBMC subsets. Together with tissue-by-tissue analysis, we also utilized Meta-Tissue software (Sul et al., 2013), a linear mixed model that allows for heterogeneity in effect sizes across conditions, for a meta-analysis across SFs under 10 stimulatory conditions and 5 PBMC subsets. When we analyzed RA and OA samples separately, the eQTL effect sizes showed high similarities between RA and OA samples. To overcome the issue of modest sample sizes, we jointly analyzed the RA and OA samples for the following

analyses. We considered variants with FDR < 0.1 in single tissue analysis or *m*-value > 0.9 in meta-analysis as significant eQTLs in line with previous reports (Gamazon et al., 2018; Sul et al., 2013).

As a result, 3245 - 4118 genes in SFs and 2557 - 2828 genes in PBMCs had significant eQTLs under each condition (Figure S2A). In total, 6962 genes in SFs and 5043 genes in PBMCs had eQTLs in at least one condition, and 2368 genes showed eQTL effects only in SFs (Figure S2B). We note that a substantial fraction of SF-specific eQTLs might be a consequence of low statistical power due to limited sample size. However, we observed a distinguishable pattern of eQTLs in SFs from that of PBMCs when comparing the effect sizes in meta-analysis (Figure S2C), indicating a tissue-wise difference of eQTL effects. When we focused on the effect size difference between stimulating SFs, the 8-mix showed the smallest correlation coefficients compared with other conditions (Figure S2C).

Next, we examined candidate causal genes among GWAS loci in SFs. We focused on eQTL variants with minimum *P* values in each associated eGene with meta-analysis or single tissue analysis, which are in linkage disequilibrium (LD) with GWAS top-associated loci of RA. Notably, various overlapped loci were observed in SFs (Table S1). One example is rs6074022, which is in tight LD (r^2 = 0.95 in EUR population, r^2 = 0.9 in EAS population) with an established RA risk locus rs4810485 (Raychaudhuri et al., 2008). By plotting eQTL meta-analysis posterior probability *m*-values and tissue-by-tissue analysis -$\log_{10}$ *P* values, rs6074022 had robust eQTL effects on *CD40* in SFs, especially under 8-mix or IFN-γ stimulatory conditions (Figure 3A, 3D). Importantly, the presence of an active regulatory region at rs6074022 was inferred only under these stimulatory conditions (Figure 3B). Although *CD40* is also expressed by B cells (Figure 3C) and known to be crucial for B cell activation as a costimulatory protein (Karnell et al., 2019), the eQTL effect at this locus was not observed in B cells in our study.

The biological role of the CD40-CD40L pathway in SFs has been discussed previously (Cho et al., 2000; Cho et al., 2007; Kim et al., 2007). However, it has not been fully explained. We performed transcriptomic analysis of RASFs stimulated with a 2-trimer form of the CD40 ligand and IFN-γ. As a result, some chemokines (e.g., *CCL5*, *CXCL10*) and cytokines (e.g., *IL6*) were significantly upregulated by the ligation of CD40L (Figure 3E). Taken together, we conjecture that CD40 upregulation in stimulated SFs is influenced by genetic predisposition, and the CD40-CD40L pathway might have a pathogenic role in RASFs.

Additional eQTL results in SFs, including *COG6* and *FAM213B,* both of which are in an RA GWAS-associated region, show eQTL effect size heterogeneity under stimulation. *CD300E, SLAMF1* and *TRAF2*, which show stimulation specificity in eQTL effects, are

shown in Figure S3. The eQTL variant list is available at the National Bioscience Database Center (NBDC) with the accession codes hum0207.v1.eQTL.v1.

Genetic risks of RA accumulate in the transcriptomic and epigenomic perturbations induced by multiple cytokines

Next, in order to elucidate the link between RA genetic risks and transcriptomic perturbations of SFs induced by various inflammatory conditions, we performed gene-set analysis with RA-associated genetic loci using MAGMA software (de Leeuw et al., 2015), which computes gene-level trait association scores and perform gene-set enrichment analysis of some gene sets with neighboring genes in the risk loci. This analysis indicated that perturbed gene sets subject to IFN-α, IFN-γ and 8-mix cytokine stimulation significantly overlapped with RA risk loci ($P = 2.0 \times 10^{-4}$, 1.7×10^{-4} and 8.3×10^{-6}, respectively). Those data contrasted with the non-significant association of transcriptome differences between RA and OA with RA genetic risk (Figure S4A, S4B). These findings indicate that there is an accumulation of RA risk loci in the pathways that are perturbed under specific stimulatory conditions in SFs from the perspective of transcriptomics.

We also assessed the enrichment of RA top risk SNPs in regulatory regions including super-enhancers (SEs) identified with ChIP sequencing. While the epigenomic mapping consortium “Roadmap” has constructed a public database of human epigenome data (http://www.roadmapepigenomics.org/), which is a fundamental resource for disease-epigenome association analysis, few epigenomic data for SFs under stimulatory conditions are publicly available. SEs are large clusters of transcriptional enhancers collectively bound by an array of transcription factors to drive expression of genes that define cell identity (ENCODE Project Consortium, 2012; Hnisz et al., 2013; Kundaje et al., 2015; Loven et al., 2013; Parker et al., 2013; Whyte et al., 2013). It is now known that disease-associated variants are enriched in the SEs of disease-relevant cell types. Although the significant overlap of SEs in Th cells and B cells with RA risk loci has been reported (Hnisz et al., 2013), SFs have not been examined. Here we divided active enhancers into SEs and typical-enhancers (TEs) following standard ROSE algorithms (Whyte et al., 2013) and compared the enrichment of RA risk loci to epigenomic marks. Consistent with previous reports (Hnisz et al., 2013), RA risk loci showed significant enrichment with SEs in $CD4^+$ T cells and B cells, as well as with SEs in 8-mix stimulated SFs from RA or OA samples (Figure 4A). SEs formed under different stimulatory conditions showed modest overlap with RA risk loci. In contrast, 8-mix cytokine treatment showed the largest unique SE overlap with some of the RA risk loci. (Figure 4B, Figure 4C). When we performed a similar comparison of our epigenomic data and risk loci for type 1 diabetes mellitus (a representative example of

non-articular autoimmune disease), only SEs in $CD4^+$ T cells and B cells showed significant enrichment (Figure S4C). The number or width of 8-mix SEs were not different from those in non-stimulated or single cytokine stimulating SFs in total (Figure S5). Consequently, SFs might behave as key players in RA pathogenesis especially under synergistic inflammation.

SEs induced by cytokine mixtures regulate genes crucial for RA pathogenesis.
Following the results above, we attempted to elucidate the genes regulated by 8-mix-enhanced SEs. SEs are not necessarily located adjacent to transcription start sites (TSS). In fact, they may lie more than 50 kb away from the TSS (Khan et al., 2018). First, to characterize the genes controlled by SEs, we combined the 3D genome architectures (chromatin loops detected by Hi-C analysis), the position of SEs, promoter regions (defined with H3K4me3 ChIP sequencing analysis) and genomic coordinates (Figure 5A). We annotated “SE-contacted genes” such that one side of Hi-C loop anchors overlapped a SE, the other side of the loop coincided with the TSS of the gene and coexisted with the H3K4me3 peak. SEs were more highly overlapped with Hi-C loop anchors than were TEs or H3K4me1 peaks (Figure S6A). H3K4me3 peaks also showed significant enrichment in Hi-C loop ends. When the gene TSS and H3K27ac peak was connected by a Hi-C loop, the variation of mRNA expression showed a significant correlation with the H3K27ac peak variation (Figure S6B). These results underscore the validity of connecting active enhancer marks and TSS by Hi-C loops in our dataset, as other reports have shown (Delaneau et al., 2019; Mumbach et al., 2017). When we compared the expression level of SE-contacted genes and TE-contacted genes, the former showed significantly higher expression levels than the latter (Figure S6C), consistent with previous reports (Whyte et al., 2013).

Next, we compared genes contacted by either SEs or TEs of SFs under 3 different conditions: nonstimulated SFs or those that were TNF-α-activated or stimulated by the mix of 8 factors. The proportions of overlap between the 3 conditions were smaller in SE-contacted genes (9.7%) than TE-contacted genes (14.5%) (Figure 5B), indicating that the stimulation-specific gene expression profile and SEs formation. SE-contacted genes included a number of transcription factors (e.g., *MTF1, RUNX1*) and genes reported to play pathogenic roles in RA such as chemokines (e.g., *CCL5, CCL8*) and cytokines (e.g., *IL6*) (Figure 5B, Table S2).

IL6 is a representative example of an 8-mix SE-contacted gene. Although this gene is regulated by a SE (almost 30 kb long) that exists upstream of the TSS in non-stimulated or TNF-α stimulated SFs, this SE elongates to 70 kb long under 8-mix conditions and an additional Hi-C loop emerges (Figure 6A). As previously mentioned, *IL6* expression is markedly upregulated under 8-mix conditions (Figure 2C), and when we inhibited SE

formation with JQ1, a BRD4 inhibitor, the increased *IL6* expression under 8-mix conditions was reduced in a dose-dependent manner (Figure 6B). The necessity of SEs for elevated IL-6 production under synergistic inflammation could be inferred from these findings.

Another example of an 8-mix SE-contacted gene is *Runt related transcription factor 1* (*RUNX1*) (Figure 6C). *RUNX1* is a master-regulator transcription factor involved in normal and malignant hematopoiesis and in T-cell acute lymphoblastic leukemia. *RUNX1* is involved in the expression of critical oncogenes (e.g., *TAL1*) by binding to their SEs with other components of the leukemogenic transcriptional complex (e.g., *MYB*) (Bahr et al., 2018; Mansour et al., 2014; Mill et al., 2019). Additionally, the binding motif of *RUNX1* was enriched in SEs of synovial fluid-derived $CD4^+$ T cells from juvenile idiopathic arthritis patients (Peeters et al., 2015). In our study, RA risk locus rs8133843 overlapped with the 8-mix SE that exists upstream of *RUNX1*. A Hi-C loop was formed with the promoter immediately above the second exon of *RUNX1* only in 8-mix conditions, and the *RUNX1* expression level was higher in the 8-mix condition compared with others.

Metal-regulatory transcription factor-1 (*MTF1*), a zinc finger transcription factor, which was reported to be an essential catabolic regulator of OA pathogenesis and tumor progression (Kim et al., 2014; Murphy, 2004), is another example of an 8-mix SE-contacted gene (Figure 6E). *MTF1* expression was upregulated in the 8-mix condition (Figure 6F). RA risk locus rs28411352 overlapped with an 8-mix SE that exists upstream of the *MTF1*. The Hi-C loop was detected with the promoter only under the 8-mix condition.

Transcription factors associated with SE formation in the presence of multiple cytokines,

Finally, we searched for candidate modulators that were crucial for SE formation, especially in the 8-mix condition. In the previous report, key transcription factors for SE formation were reported to be controlled by SEs themselves, forming a self-regulatory network (Whyte et al., 2013). From this perspective, we used motif analysis to focus on SE-contacted transcription factors that were also enriched in SEs under the 8-mix condition and compared them with TEs or SEs in the absence of stimulation (Figure 7A). Among SE-contacted genes, transcription factors such as SNAI1, TCF4 and MTF1 showed significant motif enrichment in 8-mix SEs. MTF1 was the only example that also showed the overlap of 8-mix SE and RA GWAS risk variant as discussed above (Figure 6E). Although the RUNX1 motif was not enriched in 8-mix SEs compared with unstimulated SEs, its motif was significantly enriched in SEs compared with the background sequence, both in 8-mix conditions and without stimulation ($P = 1.0 \times 10^{-16}$ and 1.0×10^{-20}, respectively). When these transcription factors in RASFs were silenced with siRNAs, the expression of 8-mix SE-contacted genes was

significantly suppressed by *MTF1* and *RUNX1* knockdown ($P = 2.0 \times 10^{-3}$ and 4.3×10^{-4}, respectively) (Figure 7B, Figure S7). The effect of *MTF1* knockdown was more pronounced in 8-mix SE-contacted genes than TE-contacted genes. These results indicated that certain transcription factors, including MTF1 and RUNX1, play critical roles in the formation of inflammation–associated epigenomic structures in the presence of synergistic cytokines.

Discussion

In this study, we conducted integrated analyses of SFs from Japanese RA and OA patients. The cells were stimulated with a variety of proinflammatory cytokines to examine epigenomic and transcriptomic responses. In that fashion, we were able to describe the dynamic landscape of SFs and their contribution to RA pathogenesis. SFs under the influence of synergistic cytokines exhibited a distinct transcriptome signature characterized by high expression of pathogenic genes (e.g., *IL6*, *MMP3*, *CSF2*). These findings were in line with the reported synergistic inflammatory responses of SFs to leukocyte-derived cytokines (TNF-α and IL-17). For example, specifically induced modulators (CUX1 and IκBζ) engage the NF-κB complex to upregulate certain chemokines (Slowikowski et al., 2019).

Recent large-scale eQTL studies have analyzed the function of non-coding variants (Battle et al., 2017; Lappalainen et al., 2013), and they have enhanced our understanding of complex diseases. However, many studies have stressed the importance of studying disease-relevant tissues for functional understanding of GWAS variants (Gamazon et al., 2018; Wainberg et al., 2019). In the present report, we expanded previous eQTL studies through analyses of SFs, which are major local effector cells in arthritic joints. Using cis-eQTL analysis, we observed thousands of associated eGenes in SFs, some of which showed the heterogeneous sizes of effects under different stimulatory conditions. One example was the association of an RA risk locus (rs4810485) with *CD40* expression. Although no significant eQTL effects of this locus in B cells was observed in our data, a previous report showed the protein-level QTL association of CD40 in $CD19^+$ B cells and this locus in European seropositive RA patients and controls (Li et al., 2013). On the contrary, a larger eQTL study by the GTEx consortium that showed genome-wide significant eQTL effects of rs6074022 on CD40 in lung (mainly fibroblasts) ($P = 3.1 \times 10^{-26}$) and cultured fibroblasts ($P = 8.4 \times 10^{-16}$), but not in EBV-transformed lymphocytes ($P = 0.04$). The subtle gap in results could be derived from racial differences of study populations and study design. Naturally, the possible importance of CD40 signals in B cells for RA pathogenesis cannot be neglected, our result of eQTL analysis and functional study in SFs might shed light on the importance of CD40-CD40L signals in SFs for RA pathogenesis. The other example of eQTL-eGene pairs in SFs was rs7993214-*COG6*. The association of this locus and

autoimmune diseases (RA, juvenile idiopathic arthritis and psoriasis) has been established (Hinks et al., 2013; Liu et al., 2008). The top eQTL variant of *COG6* in 8-mix-stimulated SFs or monocytes (rs7993214) was in tight LD with the GWAS top variant (rs9603616, r^2 = 0.93 in EUR population, r^2 = 0.82 in EAS population), and eQTL effects became more significant in stimulated SFs than in non-stimulated conditions. Upregulation of *COG6* in stimulated SFs and monocytes might play a pathogenic role in these arthritic diseases.

The significance of synergistic interactions between proinflammatory cytokines and SFs is supported by the observed accumulation of RA genetic risk loci as shown by transcriptomic and epigenomic data obtained under specific stimulatory conditions. The concept of SEs is now widely recognized. They control molecules that have prominent roles in cell type-specific processes (Loven et al., 2013; Whyte et al., 2013), and are hotspots for disease susceptibility (ENCODE Project Consortium, 2012; Hnisz et al., 2013; Kundaje et al., 2015; Parker et al., 2013). The GWAS-SEs enrichment analysis shows that SFs can behave as pathogenic cells in the development of RA (analogous to $CD4^+$ T cells and B cells) especially when exposed to the synergistic activity of proinflammatory cytokines. Note that the positions of SEs are highly flexible, and they can shift during cell differentiation or activation (Brown et al., 2014; Hah et al., 2015; Schmidt et al., 2016). Indeed, we found that SEs in SFs shifted during stimulation. The significant enrichment of RA risk SNPs in the SEs in SFs under 8-mix stimulation suggests that susceptibility regions could be exposed to the transcriptional machinery. Thus, shifting SEs could contribute to inflammatory cell-specific gene expression. Furthermore, recent fine chromatin contact maps revealed that SEs are in close proximity to the promoter of the gene they activate (Dowen et al., 2014; Hnisz et al., 2016; Ji et al., 2016; Kieffer-Kwon et al., 2013). During synergistic cytokine stimulation, Hi-C analysis suggested that there were dynamic conformational changes in three-dimensional structures involving SEs and the promoter of pathological molecules (i.e., cytokines, chemokines and transcription factors). We found marked expression of 8-mix stimulated SE-contacted genes (i.e., *IL6*, *RUNX1*, *MTF1*). This finding is compatible with a recent report describing the relationship between chromatin contact loops and gene expression level (Greenwald et al., 2019).

SEs can collapse when their co-factors are perturbed (Chapuy et al., 2013; Loven et al., 2013). Those cofactors include BET family members (Brd2, Brd3, Brd4 and Brdt) that bind to acetylated lysines in histone tails and transcription factors. In cancers that acquire SEs to drive expression of prominent oncogenes (Chapuy et al., 2013; Loven et al., 2013), BRD4 inhibitors (i.e., JQ1) ameliorated tumor progression *in vitro* and *in vivo* (See et al., 2019). Moreover, in autoimmune diseases, JQ1 preferentially inhibited the expression of SE-regulated disease-contacted genes in synovial-fluid-derived $CD4^+$ T cells from juvenile

idiopathic arthritis patients (Peeters et al., 2015). BRD4 silencing also reduced cytokine secretion, migration and invasion activity of RASFs, and JQ1 ameliorated arthritis in a collagen-induced arthritis model (Zhang et al., 2015). On the other hand, selective modulation of SEs that preferentially target disease-associated SEs in a cell type-specific manner may have better safety profiles than pan-SEs inhibitors (i.e., JQ1). In T cell leukemias, a small monoallelic insertion creates binding motifs for the master transcription factor MYB, which trigger SEs initiation upstream of oncogenes (Mansour et al., 2014). In endothelial cells, TNF-α-driven SE formation is nucleated by a single binding event of NF-κB (Brown et al., 2014). These findings suggest the potential application of SE-targeted therapies for immune-mediated diseases by selective inhibition of transcription factors.

In the present study, we analyzed transcription factors that have the potential to be selective SE modulators in SFs when stimulated by multiple synergistic proinflammatory cytokines. Given the SE-contacted genes under 8-mix stimulation and the motif enrichment, we narrowed down candidate molecules to MTF1, SNAI1, TCF4 and RUNX1. The *in vitro* knockdown assay revealed that silencing of *MTF1* or *RUNX1* significantly suppressed SE-contacted genes in the presence of 8 cytokines. Moreover, the effect of *MTF1* silencing was more prominent in 8-mix SE-contacted genes than TE-contacted genes. Those results suggest that MTF1 participates in SE formation, putatively making a feedback loop to maintain the epigenomic machinery. MTF1, a zinc finger transcription factor, regulates gene expression by binding to the metal regulatory element (MRE) within the promoter of downstream genes, in response to zinc and various stresses (Gunther et al., 2012). In the setting of disease, MTF1 could contribute to tumor metastasis and chemoresistance through the activation of the epithelial-mesenchymal transition (EMT) in some cancer cells (Ji et al., 2018). Certainly, MTF1 is highly expressed in malignancies (Shi et al., 2010), and has been reported to be a potential marker of poor prognosis (Pavon et al., 2016). Given the indicated association between EMT and the invasive phenotype of SFs (Lauzier et al., 2016), MTF1 inhibition could modify the tumor-like phenotype of SFs. Previously, the zinc-ZIP8-MTF1 axis was identified as a catabolic regulator of cartilage destruction (Kim et al., 2014). In OA chondrocytes, the Zn^{++} importer ZIP8 is specifically upregulated, and the resulting Zn^{++} influx activates MTF1, thereby enhancing the expression of matrix-degrading enzymes. Furthermore, intra-articular injection of adenovirus expressing-MTF1 in an experimental mouse model of OA promoted the expression of various matrix-degrading enzymes, cytokines and chemokines in SFs. This evidence supports the essential role of MTF1 as a bridge between joint destruction and inflammation.

There are some limitations of this study. First, the number of patients included in the cis-eQTL analysis was limited owing to sample accessibility, resulting in putatively large

false negatives. Increased sample size could better reveal the genetic influences on stimulated SFs. Second, SFs were purified by a conventional method, that is, serial passage. Previous reports showed that passage number could affect the epigenome and transcriptome of SFs (Galligan et al., 2007; Whitaker et al., 2013). To minimize the impact of culture, we restricted our analysis to early passage cells. Third, PBMCs in the present study were freshly isolated by flow cytometry and were not artificially stimulated with cytokines *ex vivo*. Thus, it is not clear whether the eQTL difference between SFs and PBMCs is attributable to cell type difference. However, over 80% of RA patients had moderate to high disease activity at the time of blood sampling, indicating that PBMCs were subject to a proinflammatory environment.

Overall, our findings shed light on SFs and their role in RA heritability. We also examined the conformational dynamics of chromatin fibers as related to the amplification of inflammation given a genetic predisposition. Our data suggest the concept of SF-targeted therapy from the perspective of epigenome remodeling. Transcription factors (MTF1, RUNX1) preferentially recruited to SEs during exposure to multiple synergistic proinflammatory cytokines would constitute novel drug targets.

Acknowledgments

We would like to thank G Inoue, M Abe, K Myouzen and K Kobayashi for their technical assistance at the Laboratory for Autoimmune Diseases, and Dr. Y Momozawa and Dr. M Kubo for providing technical advice at the Laboratory for Genotyping Development, RIKEN. We received generous support from all the physicians who participated in sample collection at the Department of Orthopaedic Surgery, the University of Tokyo.

This research was supported by funding from Takeda Pharmaceutical Co., Ltd. (Y. Kochi., K. Y. and K.F.), the Ministry of Health, Labour and Welfare, Ministry of Education, Culture, Sports, Science and Technology KAKENHI Grant-in-Aid for Scientific Research (B) (18H02846) and Grant-in-Aid for Scientific Research (C) (17K09972) from the Japan Society for the Promotion of Science.

Author Contributions

H.T., S.S., K.I., Y. Kochi., K.Y. and K.F. designed the research project. M.O. conducted bioinformatics analysis on the advice of K.I.. A.S. performed RNA sequencing. H.T. performed ChIP sequencing and other *in vitro* experiments. T.S. and K.S. performed Hi-C. H.T., Y.T., H.I., J.H., Y. Kadono. and S.T. contributed human samples. S.S. performed figure editing. H.T. and M.O. wrote the manuscript with critical inputs from Y. Kochi., K.Y. and K.F..

Declaration of Interests

The authors declare no competing financial interests.

Figure titles and legends

Figure 1. Experimental design for Integrative analysis of stimulated synovial fibroblasts from rheumatoid arthritis and osteoarthritis patients.

Our study design included SFs stimulated by 8 different factors plus a combination of all the factors. Specifically, cells were treated for 24 h with one of the following: IFN-α 100 U/mL, IFN-γ 200 U/mL, TNF-α 10 ng/mL, IL-1β 10 ng/mL, IL-6/sIL-6R 200 ng/mL, IL-17 10 ng/mL, TGF-β1 10 ng/mL or IL-18 100 ng/mL or 8-mix, a mixture of the above 8 cytokines. In addition, we used 5 freshly isolated PBMC populations ($CD4^+$ T cells, $CD8^+$ T cells, B cells, NK cells, monocytes) from the same patient cohort. RNA sequencing of individual samples from RA and OA patients (n=30 per each) was carried out, and ChIP sequencing and Hi-C analysis were conducted with pooled samples. SNP genotyping array was performed in all patients.

SFs, synovial fibroblasts; PBMCs, peripheral blood mononuclear cells; RA, rheumatoid

arthritis; OA, osteoarthritis; NS, non-stimulated.

Figure 2. The mixture of 8 cytokines induced a distinctive transcriptome signature in SFs.

(A) Principal Component Analysis (PCA) of gene expression levels for the top 1000 variable genes. Samples projected onto PC1/PC2 (left) or PC3/PC4 (right). Numbers in parentheses indicate contribution ratio (percentage of variation) of the first 4 PCs. Arrows link the centroid of indicated groups and adjusted to start from the origin.

(B) Summary of PCA for top 1000 variable genes. We fit a linear model to each PC (i.e., PC ~ Disease + Stimulation). Then we transformed the *P* values to normal Z-scores.

(C) Transcript abundances of representative RA pathogenic genes (*IL6*, *MMP3* and *CSF2*) from RNA sequencing data in stimulated SFs. Boxes, interquartile range; whiskers, distribution; dots, outliers.

PCA, principal component analysis; RA, rheumatoid arthritis; OA, osteoarthritis; NS, non-stimulated; CPM, count per million.

See also Figure S1.

Figure 3. Stimulation-specific function of RA genetic risk loci.

(A) A dot plot of rs6074022-*CD40* cis-eQTL meta-analysis posterior probability *m*-values versus tissue-by-tissue analysis -$\log_{10}$ *P* value. The gray solid line (*m*-value = 0.9) corresponds to the significance threshold in this study.

(B) Transcriptional regulatory regions around the *CD40* gene and positional relationship of rs6074022 (blue triangle) in stimulating SFs and PBMCs. IRF1 biding sites were obtained from the public epigenome browser ChIP-Atras. Data were visualized using the Integrative Genomics Viewer (IGV).

(C) Transcript abundance of *CD40* from RNA sequencing data in stimulated SFs and PBMCs. Boxes, interquartile range; whiskers, distribution; dots, outliers.

(D) Expression of *CD40* in SFs stimulated by the 8-cytokine mixture (left) and B cells (right) from each individual plotted according to the rs6074022 genotype. Nominal *P* values in eQTL mapping are shown. Boxes, interquartile range; whiskers, distribution; dots, outliers.

(E) A volcano plot of differential gene expression analysis comparing the presence or absence of CD40 ligand (CD40L) for IFN-γ-stimulated SFs. Orange and blue points mark the genes with significantly increased or decreased expression respectively for the addition of CD40L (FDR <0.01).

RA, rheumatoid arthritis; OA, osteoarthritis; NS, non-stimulated; CPM, count per million.

See also Figures S2, Figure S3 and Table S1.

Figure 4. SFs treated with 8 cytokines: super-enhancers were associated with genetic risk in RA.

(A) Enrichment of RA risk loci in transcriptional regulatory regions of stimulated SFs and PBMCs. Active enhancers were classified into super-enhancers (SEs) and typical-enhancers (TEs) following standard ROSE algorithms. The red solid lines ($-\log_{10}$ (*P* value) = 3.2) and the black solid lines ($-\log_{10}$ (*P* value) = 1.3) are the cutoffs for Bonferroni significance and nominal *P* = 0.05, respectively.

(B) A circus plot showing the overlap of SEs in SFs under different stimulatory conditions. Only the regions unique to each condition or common to all of the conditions are depicted.

(C) A circus plot showing the overlap of RA risk loci and SEs in SFs under different stimulatory conditions.

NS, non-stimulated; SE, super-enhancer; TE, typical enhancer.

See also Figures S4 and Figure S5.

Figure 5. SFs treated with 8 cytokines: SEs regulates genes crucial for RA pathogenesis.

(A) A schematic image of “SE-contacted genes”.

(B) A Venn diagram representing the overlap of TE-contacted (top) or SE-contacted (bottom) genes in SFs under different stimulatory conditions. Red, blue and black text highlight genes whose contacted SEs overlap with RA risk loci, cytokines and chemokines and transcription factors, respectively.

TSS, transcriptional start site; NS, non-stimulated; SE, super-enhancer; TE, typical enhancer.

See also Figures S6A, S6B and Table S2.

Figure 6. Representative SE-contacted genes in SFs treated with 8 cytokines.

(A, C, E) Organization of transcriptional regulatory regions around *IL6* (A), *RUNX1* (C) and *MTF1* (E) genes and positional relationship of RA risk loci (blue triangle, rs8133848 for *RUNX1* and rs28411352 for *MTF1*) and chromatin conformation in stimulated SFs. Data were visualized using the Integrative Genomics Viewer (IGV).

(B) Expression of *IL6* by SFs stimulated by 8 cytokines. SFs quantified by qRT-PCR (n = 5) treated with JQ1 (0-5000 nM) for 24 h. Expression was normalized to abundance of *GAPDH* control. Boxes, interquartile range; whiskers, distribution. *P* values were determined using one-way ANOVA followed by Tukey’s multiple comparison test (*, $P < 0.05$).

(D) Transcript abundances of *RUNX1* isoform (RUNX1b) from RNA sequencing data for

stimulated SFs and PBMCs. Boxes, interquartile range; whiskers, distribution; dots, outliers.
(F) Transcript abundances of *MTF1* from RNA sequencing data for stimulated SFs and PBMCs. Boxes, interquartile range; whiskers, distribution; dots, outliers.
RA, rheumatoid arthritis; OA, osteoarthritis; NS, non-stimulated; TPM, transcripts per million; CPM, count per million; SE, super enhancer.
See also Figures S6C.

Figure 7. Transcription factors associated with SE formation in cytokine-treated SFs.
(A) Table depicts transcription factor binding motifs enriched at SEs in SFs stimulated as follows: 8-mix, TNF-α or non-stimulated. Following are summarized: attribution to SE-contacted genes, relative enrichment *P* values to TEs in each stimulatory condition or to SEs of non-stimulated condition.
(B) Expression of SE- or TE-contacted genes in SFs stimulated by 8 cytokines in cells depleted of specified transcription factors (*TCF4*, *SNAI1*, *MTF1* and *RUNX1*) relative to control SFs. Boxes, interquartile range; whiskers, distribution. *P* values were calculated using a paired t test (*, $P < 0.05$, **, $P < 0.001$).
NS, non-stimulated; SE, super enhancer; TE, typical enhancer.
See also Figures S7.

STAR Methods

CONTACT FOR REAGENT AND RESOURCE SHARING

Further information and requests for resources and reagents should be directed to and will be fulfilled by the Lead Contact, K.F.. (kfujio-tky@umin.ac.jp).

METHOD DETAILS

Patients and sample collection

Synovial tissues were obtained from RA and OA patients (n = 30 each) undergoing joint replacement surgery at the University of Tokyo Hospital, Japan. RA patients fulfilled the 2010 ACR/EULAR (American College of Rheumatology/European League Against Rheumatism) criteria for the classification of RA (Aletaha et al., 2010). Patient characteristics are summarized in Table S4. This study was approved by the Ethics Committees of the University of Tokyo (G3582), RIKEN and the indicated medical institutions. Written informed consent was obtained from each subject in accordance with the Declaration of Helsinki. Fresh synovial tissues were minced and digested with 0.1% collagenase (Worthington) at 37℃, in 5% CO_2 for 1.5 h and SFs were cultured in Dulbecco's modified Eagle's medium (DMEM; SIGMA) supplemented with 10% fetal bovine serum

(FBS; BioWest), 100 µg/mL L-glutamine, 100 U/mL penicillin, 100 µg/mL streptomycin (all from Invitrogen). SFs from passage 2 or 3 were used for RNA sequencing, ChIP sequencing, Hi-C and functional studies after removal of macrophages by magnetic separation with CD14 microbeads (Miltenyi Biotec). The purity of SFs was tested by flow cytometry analysis (MoFlo XDP; Beckman Coulter). SFs were stained with CD14-, Thy-1 (CD90)-specific monoclonal antibodies (clone IDs: M5E2, 5E10, respectively, all from BioLegend). Most cells (>99%) had the surface marker for fibroblasts (Thy-1) but not CD14.

We collected peripheral blood from the same patients. PBMCs were isolated using Ficoll-Paque density gradient centrifugation followed by staining with CD3-, CD4-, CD8-, CD14-, CD19-, and CD56-specific monoclonal antibodies (clone IDs: UCHT1, OKT4, RPA-T8, M5E2, HIB19 and HCD56, respectively, all from BioLegend). Five immune cell populations were sorted by flow cytometry (MoFlo XDP; Beckman Coulter) using the following gating strategy: $CD4^+$ T cells: $CD3^+CD4^+CD8^-CD19^-$; $CD8^+$ T cells: $CD3^+CD4^-CD8^+CD19^-$; B cells: $CD3^-CD19^+$; NK cells: $CD3^-CD14^-CD19^-CD56^+$; and monocytes: $CD3^-CD14^+CD19^-$. There were 3×10^5 cells in each population.

RNA sequencing

Purified SFs (2×10^4 cells/well) were seeded with DMEM (10% FBS, 100 µg/mL L-glutamine, 100 U/mL penicillin, 100 µg/mL streptomycin) into a 24-well flat-bottom plate (Corning) and incubated at 37°C, in 5% CO_2. After 12 h, one of the following was added: 100 U/mL IFN-α (HumanZyme), 200 U/mL IFN-γ, 10 ng/mL TNF-α, 10 ng/mL IL-1β, 200 ng/mL IL-6/sIL-6R, 10 ng/mL IL-17 (all PeproTech), 10 ng/mL TGF-β1 (R＆D), 100 ng/mL IL-18 (MBL). Alternatively, cells were treated with “8-mix” (a mixture of the above 8 cytokines that simulated synergistic inflammation in arthritic joints). These 8 cytokines were selected on the basis of 1) existing therapeutic targets or 2) the number of articles that reported the cytokine as pathogenic on a public database (PubMed). The cells were stimulated for an additional 24 h at 37°C, in 5% CO_2.

Total RNA from SFs and freshly sorted PBMCs was isolated using AllPrep DNA/RNA/miRNA Universal Kit (Qiagen). Libraries for RNA sequencing were prepared using TruSeq Stranded mRNA Library Prep Kit (Illumina). RNA sequencing was carried out on Illumina HiSeq 2500 (read length of 125 bp, paired end).

Bioinformatic analysis of RNA sequencing data

RNA sequencing reads were aligned to the human genome assembly hg19/GRCh37 excluding minor haplotypes, random and unknown sequences. Alignment of the reads was performed by STAR (version 2.5.3) (Dobin et al., 2013) based on the GENCODE v27

(GRCh37 version) annotation. We only utilized reads that were uniquely mapped (corresponding to a mapping quality of 255 for BAM files), and properly paired for further analysis.

Gene-level read counts were quantified with HTSeq (version 0.6.0) (Anders et al., 2015) based on the GENCODE v27, with strand-specific assay mode and the other default parameters. Transcript-level quantifications were calculated with RSEM (version 1.3.0) (Li and Dewey, 2011).

We assessed the quality of each RNA sequencing sample by calculating the mean expression correlation coefficient with other samples with the same stimulatory conditions, equivalent to D statistics as described elsewhere (GTEx Consortium, 2015). All samples satisfied more than 10 million uniquely mapped read counts. We excluded samples the D statistics of which were lower than 0.9, resulting in 29 excluded samples (4 non-stimulated, 4 in TNF-α, 3 in IFN-α, 2 in IFN-γ, 6 in IL-1β, 4 in TGF-β1, 2 in IL-17, 3 in 8-mix and 1 $CD8^+$ T cell). The remaining 856 samples were utilized for the analysis.

Differential expression analysis was performed with the edgeR package with gene-level count data. For each comparison, genes whose expression was less than 10 in more than 90% of samples were excluded. Gender was included as a covariate for all the comparative analyses. RUVseq R package (Risso et al., 2014) was utilized for finding hidden factors using 1000 nonvariable genes with conditions as negative control genes and unstimulated samples as negative control samples. Gender and 3 RUV factors were considered covariates in differential expression analysis. Genes with FDR less than 0.05 in the glml RT test implemented in edgeR were regarded as differentially expressed genes.

MAGMA software was applied for gene-set analysis of GWAS data. We utilized RA GWAS summary statistics of European ancestry (Okada et al., 2014) and performed gene set enrichment analysis following the instruction by the authors. Briefly, we carried out “gene analysis” for GWAS summary statistics using the 1000 genomes European panel for LD calculation and GENCODE V27 for gene annotation. Then we carried out “gene-set analysis” using log-fold change of gene expression between conditions as gene covariate and performed enrichment analysis.

ChIP sequencing

Purified SFs (1×10^5 cells/well) were seeded with DMEM (10% FBS, 100 µg/mL L-glutamine, 100 U/mL penicillin, 100 µg/mL streptomycin) into 6-well flat-bottom plates (Corning) and incubated at 37°C, in 5% CO_2. After 12 h, 100 U/mL IFN-α, 200 U/mL IFN-γ, 10 ng/mL TNF-α, 10 ng/mL IL-1β, 200 ng/mL IL-6/sIL-6R, 10 ng/mL IL-17, 10 ng/mL TGF-β1, 100 ng/mL IL-18 or 8-mix was added. The cells were stimulated for additional 24 h at 37°C, in

5% CO_2.

Pooled SFs and freshly sorted PBMCs from RA or OA patients (n = 20 each) were cross-linked with 1% formaldehyde for 15 min at room temperature. Chromatin was prepared from pellets of SFs (1×10^7 cells) and PBMCs (2×10^7 cells) using a CHIP-IT High Sensitivity Kit and CHIP-IT PBMC Kit (both from Active Motif), respectively. Sonication was carried out by Covaris S2 (Covaris). The shearing efficiency was analyzed by agarose gel electrophoresis after RNase treatment, reversion of crosslinking and purification of DNA. Sheared chromatin (3 µg) was immunoprecipitated using 4 µL of each rabbit polyclonal antibody (H3K4me1, H3K4me3, H3K27ac, all from Active Motif). Sheared chromatin was used as the input DNA. Immunoprecipitated DNA was quantified with the Qubit dsDNA HS Kit (Invitrogen). Libraries for ChIP sequencing were prepared using TruSeq ChIP Library Prep Kit (Illumina) with 5 ng of DNA fragments. DNA size selection (250-300 bp) was carried out by BluePippin (Sage Science). ChIP sequencing was carried out on an Illumina HiSeq 2500 (read length of 50 bp, single end).

Bioinformatics analysis of ChIP sequencing data

Sequencing reads from each ChIP sequencing sample were mapped to human genome assembly hg19/GRCh37 using Bowtie2 (Langmead and Salzberg, 2012). PCR duplicates were removed, and only uniquely mapped reads were used for peak calling. MACS 2.0 (Zhang et al., 2008) was used to detect peaks which were enriched in immunoprecipitated samples over the input. Peak calling was performed with narrow peak mode for H3K4me3 and H3K27ac and broad peak mode for H3K4me1.

NSC and RSC were calculated by cross-correlation analysis following ENCODE guidelines (Landt et al., 2012) and samples with NSC less than 1.1 or RSC less than 1 were removed from the analysis. Also, samples with <10 million effective sequence reads were removed. As a result, 4 samples (RA_CD8_H3K27ac, OA_CD8_H3K27ac, OA_IL17_H3K27ac and RA_CD8_H3K4me3) were excluded and the remaining 86 samples were utilized for further analysis.

SEs were identified with the Rank Ordering of Super-Enhancers (ROSE) algorithm (Whyte et al., 2013) based on the H3K27ac ChIP sequencing signal with default parameters.

Differentially bound peak analysis for each condition was performed with HOMER software (Heinz et al., 2010) with fold-enrichment threshold of 2 and Poisson enrichment *P* value threshold of 0.0001.

Motif enrichment analysis was performed with HOMER software (Heinz et al., 2010). As motifs of some transcription factors associated with SEs were not included in the HOMER database, we customized motif reference with MotifDb software (Shannon P, Richards M

(2019). MotifDb: An Annotated Collection of Protein-DNA Binding Sequence Motifs. R package version 1.26.0.) for SE associated genes only with *homo sapiens* data.

Library construction for Hi-C

Purchased RASFs (n = 7, Articular Engineering) were used to generate an *in situ* Hi-C library as previously described with minor modifications (Rao et al., 2014). Briefly, SFs (1×10^5 cells/well) were seeded with DMEM (10% FBS, 100 µg/mL L-glutamine, 100 U/mL penicillin, 100 µg/mL streptomycin) into 6-well flat-bottom plates and incubated at 37°C, in 5% CO_2. After 12 h, either 10 ng/mL TNF-α or 8-mix was added, and the cells were stimulated for an additional 24 h at 37°C, in 5% CO_2. Pooled SFs (2.8×10^6 cells) were cross-linked with 1% formaldehyde for 10 min at room temperature. The nuclei were permeabilized, and DNA was digested with 100 units of Mbo Ⅰ restriction enzyme (NEB). The ends of restriction fragments were labeled with biotinylated nucleotides (dATP; Invitrogen), and proximity ligation was performed. After reversal of crosslinks, ligated DNA was purified and sheared to a length of roughly 400 base pairs with Covaris S2 (Covaris), at which point ligation junctions were pulled down with streptavidin beads (Invitrogen). Sequencing libraries were prepared with a Nextera Mate Pair Sample Preparation Kit (Illumina), and sequenced using a HiSeq series (read length of 150 bp, paired-end read).

Bioinformatics analysis of Hi-C data

Sequencing reads from 3 samples were mapped to human genome assembly hg19/GRCh37 using BWA-mem which is implemented in JUICER software (ver 1.8.9) (Durand et al., 2016). Loops were called using HiCCUPS (Rao et al., 2014) software implemented in JUICER with resolution of 5 kbp, 10 kbp and 25 kbp and merged loops were used for downstream analysis.

SNP typing and imputation

Genomic DNA from whole blood was isolated using QIAamp DNA Blood Midi Kit (Qiagen). Genotyping was performed using Infinium OmniExpressExome BeadChips (Illumina).

Quality control of the genotyping data was performed using PLINK 1.90, with a SNP call rate > 0.99, HWE < 1×10^{-6} and sample call rate > 0.98. For genome-wide imputation, 595693 post-QC SNPs were pre-phased using SHAPEIT and imputation was performed using IMPUTE2 with the 1000 Genomes Phase 3 panel as reference. Post-imputation QC was performed using SNPTEST. Genotyped and imputed autosomal SNPs or indels with MAF ≥ 0.05 were used for cis-eQTL analysis (6124313 variants in total).

Cis-eQTL analysis

For cis-eQTL analysis, genes detected in at least half of the samples under at least 1 condition were included. The count per million (CPM) matrix was normalized between samples using TMM as implemented in edgeR software, normalized across samples using an inverse normal transform and normalized using PEER (Stegle et al., 2012) with 15 hidden confounders, and the residuals were used for analysis. We used QTLtools (Delaneau et al., 2017) conditional pass for tissue-by-tissue eQTL analysis. In addition, to overcome the issue of modest sample sizes, we jointly analyzed the RA and OA samples. We performed a meta-analysis across SFs in various stimulatory conditions and PBMC samples for eQTLs by utilizing Meta-Tissue software (Sul et al., 2013), a linear mixed model that allows for heterogeneity in effect sizes across conditions. Cis-eQTL analysis was performed for variants with MAF ≥ 0.05 within a 1-Mb window around each gene.

For each eQTL, we estimated the posterior probability that the effect is shared in each tissue (*m*-value) along with tissue-by-tissue eQTL analysis *P* value.

GWAS enrichment analysis

In order to calculate GWAS variant enrichment for epigenomic marks, we prepared 10,000 sets of randomly sampled variants that were matched to GWAS variants for distance from the nearest TSS, minor allele frequency (MAF), gene density and the number of LD variants ($r^2 \geq 0.5$) using SNPSNAP (Pers et al., 2015). We counted the number of GWAS variants or randomly selected variants whose LD ($r^2 \geq 0.8$) variants or itself coincided with epigenomic marks. We calculated the empirical *P* value by comparing the number of GWAS variants that tagged epigenomic marks against the number of randomly selected variants that tagged epigenomic marks. We pruned GWAS variants such that no 2 variants were within 1 Mb of one another, and all GWAS variants within the extended MHC region (25–35 Mb on chromosome 6) were removed from the analysis.

Population enrichment score

In order to assess the abundance of SF populations reported in the single-cell transcriptome based analysis (Zhang et al., 2019), we calculated the population enrichment score of each SFs sample. We used “top 20 marker genes for each single-cell RNA sequencing cluster” of 4 SF clusters from the article and calculated the enrichment score of these gene sets using GSVA software (Hanzelmann et al., 2013) with normalized CPM.

cDNA synthesis and qRT-PCR

Purified RASFs (2×10^4 cells/well) were seeded with DMEM (10% FBS, 100 μg/mL

L-glutamine, 100 U/mL penicillin, 100 µg/mL streptomycin) into 24-well flat-bottom plates and incubated at 37°C, in 5% CO^2. After 12 h, 100 U/mL IFN-α, 200 U/mL IFN-γ, 10 ng/mL TNF-α, 10 ng/mL IL-1β, 200 ng/mL IL-6/sIL-6R, 10 ng/mL IL-17, 10 ng/mL TGF-β1, 100 ng/mL IL-18, or 8-mix was added. The cells were stimulated for an additional 3, 10, 24 or 48 h at 37°C, in 5% CO_2. In *in vitro* inhibition studies of Brd4, JQ1 (Sigma; 5-5000 ng/mL) was simultaneously added with 8-mix, and incubated for an additional 3, 10, 24 or 48 h at 37°C, in 5% CO_2.

Total RNAs were extracted with RNeasy Micro Kit (Qiagen) and were reverse-transcribed to cDNA with random primers (Invitrogen), dNTP mixture (Takara), ribonuclease inhibitor (Promega) and SuperScript III (Invitrogen). Quantitative real-time PCR (qRT-PCR) was performed using CFX Connect Real-Time PCR Detection System (Bio-Rad) with QuantiTect SYBR Green PCR Kit (Qiagen). The primer pairs used in this study are shown in Table S3. Relative expression was calculated based on the abundance of control *GAPDH*.

Knockdown assay

Purchased RASFs were used for knockdown assays. Cells (4×10^5 cells/target) were transfected with 300 nM ON-TARGET plus siRNA targeting *BRD4, MTF1, RUNX1, SNAI1, SNAI2* or *TCF4* (all Dharmacon) using a Human Dermal Fibroblast Nucleofector Kit (Lonza) according to the manufacturer's instructions. SiGENOME Non-Targeting Control Pool (300 nM, Dharmacon) was used as a transfection control. Transfected cells (4×10^4 cells/well) were seeded with DMEM (10% FBS, 100 µg/mL L-glutamine, 100 U/mL penicillin, 100 µg/mL streptomycin) into 24-well flat-bottom plates and incubated at 37°C, in 5% CO_2. After 6 h, cells were stimulated with 8-mix cytokines for an additional 6 h. Total RNA was isolated using AllPrep DNA/RNA/miRNA Universal Kit. Libraries for RNA sequencing were prepared using TruSeq Stranded mRNA Library Prep Kit. mRNA sequencing was carried out on Illumina MiSeq (read length of 150 bp, paired end).

CD40 stimulation assay

Purchased RASFs (n = 3) were used in the CD40 stimulation assay. RASFs (2×10^4 cells/well) were seeded with DMEM (10% FBS, 100 µg/mL L-glutamine, 100 U/mL penicillin, 100 µg/mL streptomycin) into 24-well flat-bottom plates and incubated at 37°C, in 5% CO_2. After 12 h, cells were stimulated with 1-10 ng/mL CD40L (ENZ) and 200 U/mL IFN-γ or 8-mix for an additional 24 h. RNA extraction, cDNA synthesis and RT-PCR was performed as described above. Total RNA was isolated using AllPrep DNA/RNA/miRNA Universal Kit. Libraries for RNA sequencing were prepared using TruSeq Stranded mRNA Library Prep Kit. The mRNA sequencing was carried out on Illumina MiSeq (read length of 150 bp, paired

end).

Quantification and Statistical Analysis

For *in vitro* analysis, statistical significance and analysis of variance (ANOVA) between indicated groups were analyzed by R (ver 3.5.3). A comparison of more than 2 group means was analyzed by Tukey's multiple comparison tests. A comparison of 2 group means was analyzed by paired t-test. Statistically significant differences were accepted at $P < 0.05$ for all tests. Data in the figures were expressed as means ± SD or SEM.

DATA AND SOFTWARE AVAILABILITY

The datasets generated during this study are available at the National Bioscience Database Center (NBDC) with the study accession code hum0207 (read counts data of RNA sequencing, hum0207.v1.RNA.v1; eQTL summary, hum0207.v1.eQTL.v1; peaks data of ChIP sequencing, hum0207.v1.ChIP.v1; chromatin loops data of Hi-C, hum0207.v1.HiC.v1).

Supplemental Information titles and legends

Table S1 (Related to Figure 3). Colocalization of RA GWAS and cis-eQTL signals.

The list of cis-eQTL top variants which are in LD with RA GWAS lead variants. Variant pairs with $R^2 > 0.6$ in EUR or EAS population in 1000G phase 3 data are listed. The RA GWAS top variant was downloaded from the NHGRI-EBI GWAS Catalog (Buniello et al., 2019). EFO_0000685 was downloaded on 11/09/2018.

eQTL, expression quantitative trait locus; GWAS, lead variant in genome-wide association study; R^2, r square values between eQTL top variant and GWAS lead variant in EUR or EAS population (the larger one is written); method, eQTL analysis method for the indicated top eQTL variant; MT, meta-tissue analysis; TBT, tissue-by-tissue analysis

Table S2 (Related to Figure 5). Summary of SE-contacted genes.

References

Aho, K., Koskenvuo, M., Tuominen, J., and Kaprio, J. (1986). Occurrence of rheumatoid arthritis in a nationwide series of twins. The Journal of rheumatology *13*, 899-902.

Aletaha, D., Neogi, T., Silman, A.J., Funovits, J., Felson, D.T., Bingham, C.O., 3rd, Birnbaum, N.S., Burmester, G.R., Bykerk, V.P., Cohen, M.D.*, et al.* (2010). 2010 Rheumatoid arthritis classification criteria: an American College of Rheumatology/European League Against Rheumatism collaborative initiative. Arthritis and rheumatism *62*, 2569-2581.

Anders, S., Pyl, P.T., and Huber, W. (2015). HTSeq--a Python framework to work with

high-throughput sequencing data. Bioinformatics (Oxford, England) *31*, 166-169.

Arend, W.P., and Dayer, J.M. (1990). Cytokines and cytokine inhibitors or antagonists in rheumatoid arthritis. Arthritis and rheumatism *33*, 305-315.

Bahr, C., von Paleske, L., Uslu, V.V., Remeseiro, S., Takayama, N., Ng, S.W., Murison, A., Langenfeld, K., Petretich, M., Scognamiglio, R.*, et al.* (2018). A Myc enhancer cluster regulates normal and leukaemic haematopoietic stem cell hierarchies. Nature *553*, 515-520.

Baker, K.F., and Isaacs, J.D. (2018). Novel therapies for immune-mediated inflammatory diseases: What can we learn from their use in rheumatoid arthritis, spondyloarthritis, systemic lupus erythematosus, psoriasis, Crohn's disease and ulcerative colitis? Annals of the rheumatic diseases *77*, 175-187.

Battle, A., Brown, C.D., Engelhardt, B.E., and Montgomery, S.B. (2017). Genetic effects on gene expression across human tissues. Nature *550*, 204-213.

Brown, J.D., Lin, C.Y., Duan, Q., Griffin, G., Federation, A., Paranal, R.M., Bair, S., Newton, G., Lichtman, A., Kung, A.*, et al.* (2014). NF-kappaB directs dynamic super enhancer formation in inflammation and atherogenesis. Molecular cell *56*, 219-231.

Buniello, A., MacArthur, J.A.L., Cerezo, M., Harris, L.W., Hayhurst, J., Malangone, C., McMahon, A., Morales, J., Mountjoy, E., Sollis, E.*, et al.* (2019). The NHGRI-EBI GWAS Catalog of published genome-wide association studies, targeted arrays and summary statistics 2019. Nucleic acids research *47*, D1005-d1012.

Chapuy, B., McKeown, M.R., Lin, C.Y., Monti, S., Roemer, M.G., Qi, J., Rahl, P.B., Sun, H.H., Yeda, K.T., Doench, J.G.*, et al.* (2013). Discovery and characterization of super-enhancer-associated dependencies in diffuse large B cell lymphoma. Cancer cell *24*, 777-790.

Chen, Z., Bozec, A., Ramming, A., and Schett, G. (2019). Anti-inflammatory and immune-regulatory cytokines in rheumatoid arthritis. Nature reviews. Rheumatology *15*, 9-17.

Cho, C.S., Cho, M.L., Min, S.Y., Kim, W.U., Min, D.J., Lee, S.S., Park, S.H., Choe, J., and Kim, H.Y. (2000). CD40 engagement on synovial fibroblast up-regulates production of vascular endothelial growth factor. Journal of immunology (Baltimore, Md. : 1950) *164*, 5055-5061.

Cho, M.L., Yoon, B.Y., Ju, J.H., Jung, Y.O., Jhun, J.Y., Park, M.K., Park, S.H., Cho, C.S., and Kim, H.Y. (2007). Expression of CCR2A, an isoform of MCP-1 receptor, is increased by MCP-1, CD40 ligand and TGF-beta in fibroblast like synoviocytes of patients with RA. Experimental & molecular medicine *39*, 499-507.

de la Rica, L., Urquiza, J.M., Gomez-Cabrero, D., Islam, A.B., Lopez-Bigas, N., Tegner, J., Toes, R.E., and Ballestar, E. (2013). Identification of novel markers in rheumatoid arthritis through integrated analysis of DNA methylation and microRNA expression. Journal of autoimmunity *41*, 6-16.

de Leeuw, C.A., Mooij, J.M., Heskes, T., and Posthuma, D. (2015). MAGMA: generalized gene-set analysis of GWAS data. PLoS computational biology *11*, e1004219.

Delaneau, O., Ongen, H., Brown, A.A., Fort, A., Panousis, N.I., and Dermitzakis, E.T. (2017). A complete tool set for molecular QTL discovery and analysis. Nature communications *8*, 15452.

Delaneau, O., Zazhytska, M., Borel, C., Giannuzzi, G., Rey, G., Howald, C., Kumar, S., Ongen, H., Popadin, K., Marbach, D.*, et al.* (2019). Chromatin three-dimensional interactions mediate genetic effects on gene expression. Science (New York, N.Y.) *364*.

Dobin, A., Davis, C.A., Schlesinger, F., Drenkow, J., Zaleski, C., Jha, S., Batut, P., Chaisson, M., and Gingeras, T.R. (2013). STAR: ultrafast universal RNA-seq aligner. Bioinformatics (Oxford, England) *29*, 15-21.

Dowen, J.M., Fan, Z.P., Hnisz, D., Ren, G., Abraham, B.J., Zhang, L.N., Weintraub, A.S., Schujiers, J., Lee, T.I., Zhao, K., and Young, R.A. (2014). Control of cell identity genes occurs in insulated neighborhoods in mammalian chromosomes. Cell *159*, 374-387.

Durand, N.C., Shamim, M.S., Machol, I., Rao, S.S., Huntley, M.H., Lander, E.S., and Aiden, E.L. (2016). Juicer Provides a One-Click System for Analyzing Loop-Resolution Hi-C Experiments. Cell systems *3*, 95-98.

ENCODE Project Consortium (2012). An integrated encyclopedia of DNA elements in the human genome. Nature *489*, 57-74.

Fairfax, B.P., Humburg, P., Makino, S., Naranbhai, V., Wong, D., Lau, E., Jostins, L., Plant, K., Andrews, R., McGee, C., and Knight, J.C. (2014). Innate immune activity conditions the effect of regulatory variants upon monocyte gene expression. Science (New York, N.Y.) *343*, 1246949.

Farh, K.K., Marson, A., Zhu, J., Kleinewietfeld, M., Housley, W.J., Beik, S., Shoresh, N., Whitton, H., Ryan, R.J., Shishkin, A.A.*, et al.* (2015). Genetic and epigenetic fine mapping of causal autoimmune disease variants. Nature *518*, 337-343.

Frank-Bertoncelj, M., Klein, K., and Gay, S. (2017). Interplay between genetic and epigenetic mechanisms in rheumatoid arthritis. Epigenomics *9*, 493-504.

Galligan, C.L., Baig, E., Bykerk, V., Keystone, E.C., and Fish, E.N. (2007). Distinctive gene expression signatures in rheumatoid arthritis synovial tissue fibroblast cells: correlates with disease activity. Genes and immunity *8*, 480-491.

Gamazon, E.R., Segre, A.V., van de Bunt, M., Wen, X., Xi, H.S., Hormozdiari, F., Ongen, H., Konkashbaev, A., Derks, E.M., Aguet, F.*, et al.* (2018). Using an atlas of gene regulation across 44 human tissues to inform complex disease- and trait-associated variation. Nature genetics *50*, 956-967.

Garbers, C., Heink, S., Korn, T., and Rose-John, S. (2018). Interleukin-6: designing specific therapeutics for a complex cytokine. Nature reviews. Drug discovery *17*, 395-412.

Genovese, M.C., Cohen, S., Moreland, L., Lium, D., Robbins, S., Newmark, R., and Bekker, P.

(2004). Combination therapy with etanercept and anakinra in the treatment of patients with rheumatoid arthritis who have been treated unsuccessfully with methotrexate. Arthritis and rheumatism *50*, 1412-1419.

Greenwald, W.W., Li, H., Benaglio, P., Jakubosky, D., Matsui, H., Schmitt, A., Selvaraj, S., D'Antonio, M., D'Antonio-Chronowska, A., Smith, E.N., and Frazer, K.A. (2019). Subtle changes in chromatin loop contact propensity are associated with differential gene regulation and expression. Nature communications *10*, 1054.

GTEx Consortium (2015). Human genomics. The Genotype-Tissue Expression (GTEx) pilot analysis: multitissue gene regulation in humans. Science (New York, N.Y.) *348*, 648-660.

Gunther, V., Lindert, U., and Schaffner, W. (2012). The taste of heavy metals: gene regulation by MTF-1. Biochimica et biophysica acta *1823*, 1416-1425.

Hah, N., Benner, C., Chong, L.W., Yu, R.T., Downes, M., and Evans, R.M. (2015). Inflammation-sensitive super enhancers form domains of coordinately regulated enhancer RNAs. Proceedings of the National Academy of Sciences of the United States of America *112*, E297-302.

Hanzelmann, S., Castelo, R., and Guinney, J. (2013). GSVA: gene set variation analysis for microarray and RNA-seq data. BMC bioinformatics *14*, 7.

Heinz, S., Benner, C., Spann, N., Bertolino, E., Lin, Y.C., Laslo, P., Cheng, J.X., Murre, C., Singh, H., and Glass, C.K. (2010). Simple combinations of lineage-determining transcription factors prime cis-regulatory elements required for macrophage and B cell identities. Molecular cell *38*, 576-589.

Hinks, A., Cobb, J., Marion, M.C., Prahalad, S., Sudman, M., Bowes, J., Martin, P., Comeau, M.E., Sajuthi, S., Andrews, R.*, et al.* (2013). Dense genotyping of immune-related disease regions identifies 14 new susceptibility loci for juvenile idiopathic arthritis. Nature genetics *45*, 664-669.

Hnisz, D., Abraham, B.J., Lee, T.I., Lau, A., Saint-Andre, V., Sigova, A.A., Hoke, H.A., and Young, R.A. (2013). Super-enhancers in the control of cell identity and disease. Cell *155*, 934-947.

Hnisz, D., Weintraub, A.S., Day, D.S., Valton, A.L., Bak, R.O., Li, C.H., Goldmann, J., Lajoie, B.R., Fan, Z.P., Sigova, A.A.*, et al.* (2016). Activation of proto-oncogenes by disruption of chromosome neighborhoods. Science (New York, N.Y.) *351*, 1454-1458.

Ji, L., Zhao, G., Zhang, P., Huo, W., Dong, P., Watari, H., Jia, L., Pfeffer, L.M., Yue, J., and Zheng, J. (2018). Knockout of MTF1 Inhibits the Epithelial to Mesenchymal Transition in Ovarian Cancer Cells. Journal of Cancer *9*, 4578-4585.

Ji, X., Dadon, D.B., Powell, B.E., Fan, Z.P., Borges-Rivera, D., Shachar, S., Weintraub, A.S., Hnisz, D., Pegoraro, G., Lee, T.I.*, et al.* (2016). 3D Chromosome Regulatory Landscape of Human Pluripotent Cells. Cell stem cell *18*, 262-275.

Kang, S., Tanaka, T., Narazaki, M., and Kishimoto, T. (2019). Targeting Interleukin-6 Signaling in Clinic. Immunity *50*, 1007-1023.

Kantarjian, H., Stein, A., Gokbuget, N., Fielding, A.K., Schuh, A.C., Ribera, J.M., Wei, A., Dombret, H., Foa, R., Bassan, R.*, et al.* (2017). Blinatumomab versus Chemotherapy for Advanced Acute Lymphoblastic Leukemia. The New England journal of medicine *376*, 836-847.

Karnell, J.L., Rieder, S.A., Ettinger, R., and Kolbeck, R. (2019). Targeting the CD40-CD40L pathway in autoimmune diseases: Humoral immunity and beyond. Advanced drug delivery reviews *141*, 92-103.

Katz, Y., Nadiv, O., and Beer, Y. (2001). Interleukin-17 enhances tumor necrosis factor alpha-induced synthesis of interleukins 1,6, and 8 in skin and synovial fibroblasts: a possible role as a "fine-tuning cytokine" in inflammation processes. Arthritis and rheumatism *44*, 2176-2184.

Khan, A., Mathelier, A., and Zhang, X. (2018). Super-enhancers are transcriptionally more active and cell type-specific than stretch enhancers. Epigenetics *13*, 910-922.

Kieffer-Kwon, K.R., Tang, Z., Mathe, E., Qian, J., Sung, M.H., Li, G., Resch, W., Baek, S., Pruett, N., Grontved, L.*, et al.* (2013). Interactome maps of mouse gene regulatory domains reveal basic principles of transcriptional regulation. Cell *155*, 1507-1520.

Kim, J.H., Jeon, J., Shin, M., Won, Y., Lee, M., Kwak, J.S., Lee, G., Rhee, J., Ryu, J.H., Chun, C.H., and Chun, J.S. (2014). Regulation of the catabolic cascade in osteoarthritis by the zinc-ZIP8-MTF1 axis. Cell *156*, 730-743.

Kim, K.W., Cho, M.L., Kim, H.R., Ju, J.H., Park, M.K., Oh, H.J., Kim, J.S., Park, S.H., Lee, S.H., and Kim, H.Y. (2007). Up-regulation of stromal cell-derived factor 1 (CXCL12) production in rheumatoid synovial fibroblasts through interactions with T lymphocytes: role of interleukin-17 and CD40L-CD40 interaction. Arthritis and rheumatism *56*, 1076-1086.

Kokebie, R., Aggarwal, R., Lidder, S., Hakimiyan, A.A., Rueger, D.C., Block, J.A., and Chubinskaya, S. (2011). The role of synovial fluid markers of catabolism and anabolism in osteoarthritis, rheumatoid arthritis and asymptomatic organ donors. Arthritis research & therapy *13*, R50.

Kundaje, A., Meuleman, W., Ernst, J., Bilenky, M., Yen, A., Heravi-Moussavi, A., Kheradpour, P., Zhang, Z., Wang, J., Ziller, M.J.*, et al.* (2015). Integrative analysis of 111 reference human epigenomes. Nature *518*, 317-330.

Landt, S.G., Marinov, G.K., Kundaje, A., Kheradpour, P., Pauli, F., Batzoglou, S., Bernstein, B.E., Bickel, P., Brown, J.B., Cayting, P.*, et al.* (2012). ChIP-seq guidelines and practices of the ENCODE and modENCODE consortia. Genome research *22*, 1813-1831.

Langmead, B., and Salzberg, S.L. (2012). Fast gapped-read alignment with Bowtie 2. Nature methods *9*, 357-359.

Lappalainen, T., Sammeth, M., Friedlander, M.R., t Hoen, P.A., Monlong, J., Rivas, M.A.,

Gonzalez-Porta, M., Kurbatova, N., Griebel, T., Ferreira, P.G., *et al.* (2013). Transcriptome and genome sequencing uncovers functional variation in humans. Nature *501*, 506-511.

Lauzier, A., Lavoie, R.R., Charbonneau, M., Gouin-Boisvert, B., Harper, K., and Dubois, C.M. (2016). Snail Is a Critical Mediator of Invadosome Formation and Joint Degradation in Arthritis. The American journal of pathology *186*, 359-374.

Leech, M.T., and Morand, E.F. (2013). Fibroblasts and synovial immunity. Current opinion in pharmacology *13*, 565-569.

Li, B., and Dewey, C.N. (2011). RSEM: accurate transcript quantification from RNA-Seq data with or without a reference genome. BMC bioinformatics *12*, 323.

Li, G., Diogo, D., Wu, D., Spoonamore, J., Dancik, V., Franke, L., Kurreeman, F., Rossin, E.J., Duclos, G., Hartland, C., *et al.* (2013). Human genetics in rheumatoid arthritis guides a high-throughput drug screen of the CD40 signaling pathway. PLoS genetics *9*, e1003487.

Liu, Y., Helms, C., Liao, W., Zaba, L.C., Duan, S., Gardner, J., Wise, C., Miner, A., Malloy, M.J., Pullinger, C.R., *et al.* (2008). A genome-wide association study of psoriasis and psoriatic arthritis identifies new disease loci. PLoS genetics *4*, e1000041.

Loven, J., Hoke, H.A., Lin, C.Y., Lau, A., Orlando, D.A., Vakoc, C.R., Bradner, J.E., Lee, T.I., and Young, R.A. (2013). Selective inhibition of tumor oncogenes by disruption of super-enhancers. Cell *153*, 320-334.

Mansour, M.R., Abraham, B.J., Anders, L., Berezovskaya, A., Gutierrez, A., Durbin, A.D., Etchin, J., Lawton, L., Sallan, S.E., Silverman, L.B., *et al.* (2014). Oncogene regulation. An oncogenic super-enhancer formed through somatic mutation of a noncoding intergenic element. Science (New York, N.Y.) *346*, 1373-1377.

Mill, C.P., Fiskus, W., DiNardo, C.D., Qian, Y., Raina, K., Rajapakshe, K., Perera, D., Coarfa, C., Kadia, T.M., Khoury, J.D., *et al.* (2019). RUNX1-targeted therapy for AML expressing somatic or germline mutation in RUNX1. Blood *134*, 59-73.

Mumbach, M.R., Satpathy, A.T., Boyle, E.A., Dai, C., Gowen, B.G., Cho, S.W., Nguyen, M.L., Rubin, A.J., Granja, J.M., Kazane, K.R., *et al.* (2017). Enhancer connectome in primary human cells identifies target genes of disease-associated DNA elements. Nature genetics *49*, 1602-1612.

Murphy, B.J. (2004). Regulation of malignant progression by the hypoxia-sensitive transcription factors HIF-1alpha and MTF-1. Comparative biochemistry and physiology. Part B, Biochemistry & molecular biology *139*, 495-507.

Nakano, K., Whitaker, J.W., Boyle, D.L., Wang, W., and Firestein, G.S. (2013). DNA methylome signature in rheumatoid arthritis. Annals of the rheumatic diseases *72*, 110-117.

Okada, Y., Eyre, S., Suzuki, A., Kochi, Y., and Yamamoto, K. (2019). Genetics of rheumatoid arthritis: 2018 status. Annals of the rheumatic diseases *78*, 446-453.

Okada, Y., Wu, D., Trynka, G., Raj, T., Terao, C., Ikari, K., Kochi, Y., Ohmura, K., Suzuki, A., Yoshida, S.*, et al.* (2014). Genetics of rheumatoid arthritis contributes to biology and drug discovery. Nature *506*, 376-381.

Ospelt, C., Gay, S., and Klein, K. (2017). Epigenetics in the pathogenesis of RA. Seminars in immunopathology *39*, 409-419.

Parker, S.C., Stitzel, M.L., Taylor, D.L., Orozco, J.M., Erdos, M.R., Akiyama, J.A., van Bueren, K.L., Chines, P.S., Narisu, N., Black, B.L.*, et al.* (2013). Chromatin stretch enhancer states drive cell-specific gene regulation and harbor human disease risk variants. Proceedings of the National Academy of Sciences of the United States of America *110*, 17921-17926.

Pavon, M.A., Parreno, M., Tellez-Gabriel, M., Leon, X., Arroyo-Solera, I., Lopez, M., Cespedes, M.V., Casanova, I., Gallardo, A., Lopez-Pousa, A.*, et al.* (2016). CKMT1 and NCOA1 expression as a predictor of clinical outcome in patients with advanced-stage head and neck squamous cell carcinoma. Head & neck *38 Suppl 1*, E1392-1403.

Peeters, J.G., Vervoort, S.J., Tan, S.C., Mijnheer, G., de Roock, S., Vastert, S.J., Nieuwenhuis, E.E., van Wijk, F., Prakken, B.J., Creyghton, M.P.*, et al.* (2015). Inhibition of Super-Enhancer Activity in Autoinflammatory Site-Derived T Cells Reduces Disease-Associated Gene Expression. Cell reports *12*, 1986-1996.

Pers, T.H., Timshel, P., and Hirschhorn, J.N. (2015). SNPsnap: a Web-based tool for identification and annotation of matched SNPs. Bioinformatics (Oxford, England) *31*, 418-420.

Rao, S.S., Huntley, M.H., Durand, N.C., Stamenova, E.K., Bochkov, I.D., Robinson, J.T., Sanborn, A.L., Machol, I., Omer, A.D., Lander, E.S., and Aiden, E.L. (2014). A 3D map of the human genome at kilobase resolution reveals principles of chromatin looping. Cell *159*, 1665-1680.

Raychaudhuri, S., Remmers, E.F., Lee, A.T., Hackett, R., Guiducci, C., Burtt, N.P., Gianniny, L., Korman, B.D., Padyukov, L., Kurreeman, F.A.*, et al.* (2008). Common variants at CD40 and other loci confer risk of rheumatoid arthritis. Nature genetics *40*, 1216-1223.

Risso, D., Ngai, J., Speed, T.P., and Dudoit, S. (2014). Normalization of RNA-seq data using factor analysis of control genes or samples. Nature biotechnology *32*, 896-902.

Schmidt, S.V., Krebs, W., Ulas, T., Xue, J., Bassler, K., Gunther, P., Hardt, A.L., Schultze, H., Sander, J., Klee, K.*, et al.* (2016). The transcriptional regulator network of human inflammatory macrophages is defined by open chromatin. Cell research *26*, 151-170.

See, Y.X., Wang, B.Z., and Fullwood, M.J. (2019). Chromatin Interactions and Regulatory Elements in Cancer: From Bench to Bedside. Trends in genetics : TIG *35*, 145-158.

Shi, Y., Amin, K., Sato, B.G., Samuelsson, S.J., Sambucetti, L., Haroon, Z.A., Laderoute, K., and Murphy, B.J. (2010). The metal-responsive transcription factor-1 protein is elevated in human tumors. Cancer biology & therapy *9*, 469-476.

Silman, A.J., MacGregor, A.J., Thomson, W., Holligan, S., Carthy, D., Farhan, A., and Ollier, W.E. (1993). Twin concordance rates for rheumatoid arthritis: results from a nationwide study. British journal of rheumatology *32*, 903-907.

Slowikowski, K., Nguyen, H.N., Noss, E.H., Simmons, D.P., Mizoguchi, F., Watts, G.F.M., Gurish, M.F., Brenner, M.B., and Raychaudhuri, S. (2019). CUX1 and IκBζ mediate the synergistic inflammatory response to TNF and IL-17A in stromal fibroblasts. bioRxiv, 571315.

Slowikowski, K., Wei, K., Brenner, M.B., and Raychaudhuri, S. (2018). Functional genomics of stromal cells in chronic inflammatory diseases. Current opinion in rheumatology *30*, 65-71.

Smolen, J.S., Aletaha, D., Barton, A., Burmester, G.R., Emery, P., Firestein, G.S., Kavanaugh, A., McInnes, I.B., Solomon, D.H., Strand, V., and Yamamoto, K. (2018). Rheumatoid arthritis. Nature reviews. Disease primers *4*, 18001.

Stegle, O., Parts, L., Piipari, M., Winn, J., and Durbin, R. (2012). Using probabilistic estimation of expression residuals (PEER) to obtain increased power and interpretability of gene expression analyses. Nature protocols *7*, 500-507.

Sul, J.H., Han, B., Ye, C., Choi, T., and Eskin, E. (2013). Effectively identifying eQTLs from multiple tissues by combining mixed model and meta-analytic approaches. PLoS genetics *9*, e1003491.

Takayanagi, H. (2007). Osteoimmunology: shared mechanisms and crosstalk between the immune and bone systems. Nature reviews. Immunology *7*, 292-304.

van Vollenhoven, R. (2019). Treat-to-target in rheumatoid arthritis - are we there yet? Nature reviews. Rheumatology *15*, 180-186.

Wainberg, M., Sinnott-Armstrong, N., Mancuso, N., Barbeira, A.N., Knowles, D.A., Golan, D., Ermel, R., Ruusalepp, A., Quertermous, T., Hao, K.*, et al.* (2019). Opportunities and challenges for transcriptome-wide association studies. Nature genetics *51*, 592-599.

Whitaker, J.W., Shoemaker, R., Boyle, D.L., Hillman, J., Anderson, D., Wang, W., and Firestein, G.S. (2013). An imprinted rheumatoid arthritis methylome signature reflects pathogenic phenotype. Genome medicine *5*, 40.

Whyte, W.A., Orlando, D.A., Hnisz, D., Abraham, B.J., Lin, C.Y., Kagey, M.H., Rahl, P.B., Lee, T.I., and Young, R.A. (2013). Master transcription factors and mediator establish super-enhancers at key cell identity genes. Cell *153*, 307-319.

Zhang, F., Wei, K., Slowikowski, K., Fonseka, C.Y., Rao, D.A., Kelly, S., Goodman, S.M., Tabechian, D., Hughes, L.B., Salomon-Escoto, K.*, et al.* (2019). Defining inflammatory cell states in rheumatoid arthritis joint synovial tissues by integrating single-cell transcriptomics and mass cytometry. Nature immunology *20*, 928-942.

Zhang, Q.G., Qian, J., and Zhu, Y.C. (2015). Targeting bromodomain-containing protein 4 (BRD4) benefits rheumatoid arthritis. Immunology letters *166*, 103-108.

Zhang, Y., Liu, T., Meyer, C.A., Eeckhoute, J., Johnson, D.S., Bernstein, B.E., Nusbaum, C., Myers, R.M., Brown, M., Li, W., and Liu, X.S. (2008). Model-based analysis of ChIP-Seq (MACS). Genome biology *9*, R137.

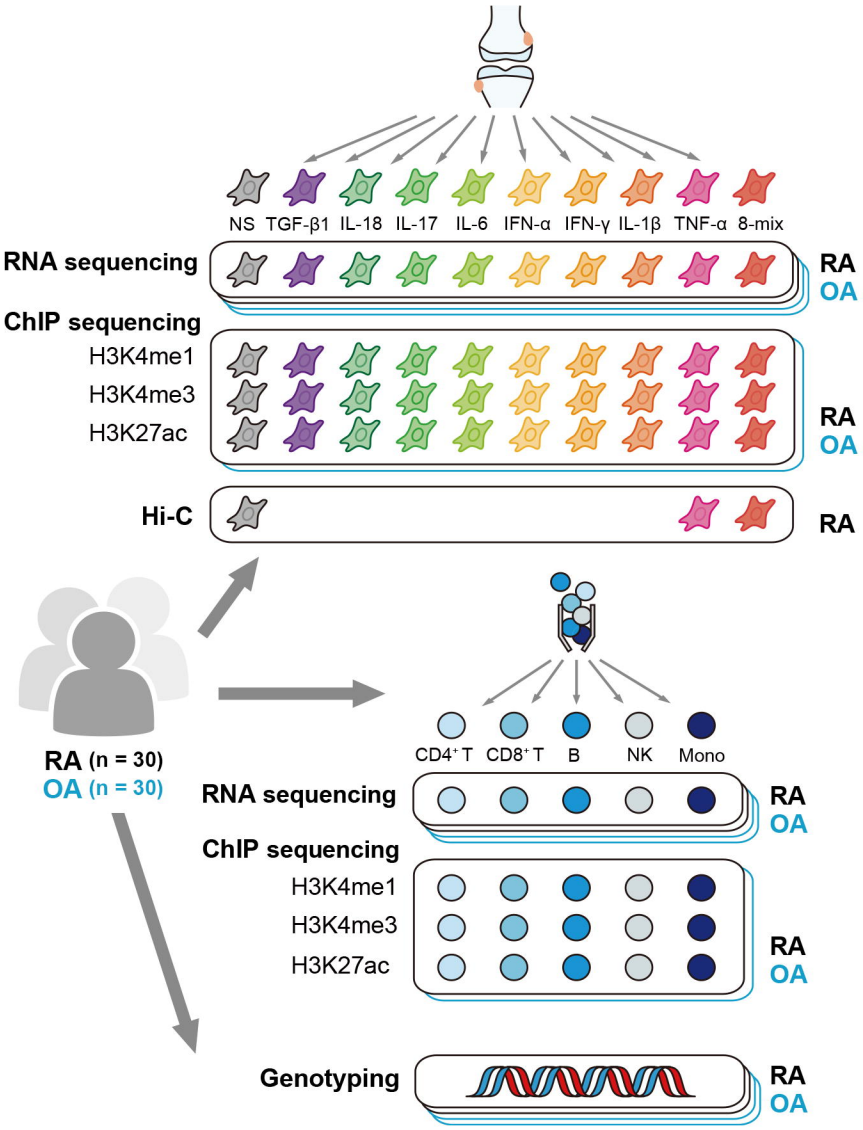

Figure 1

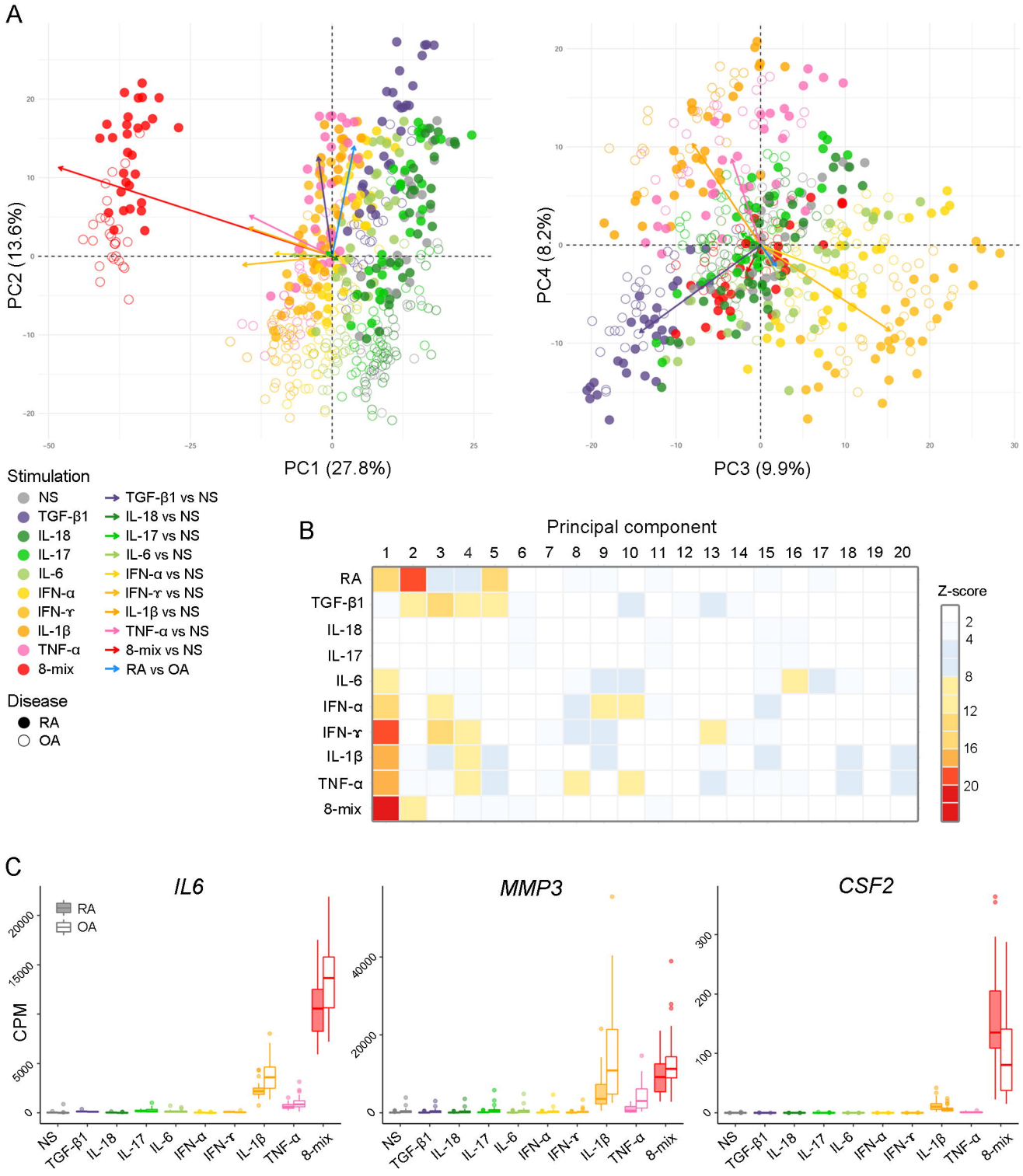

Figure 2

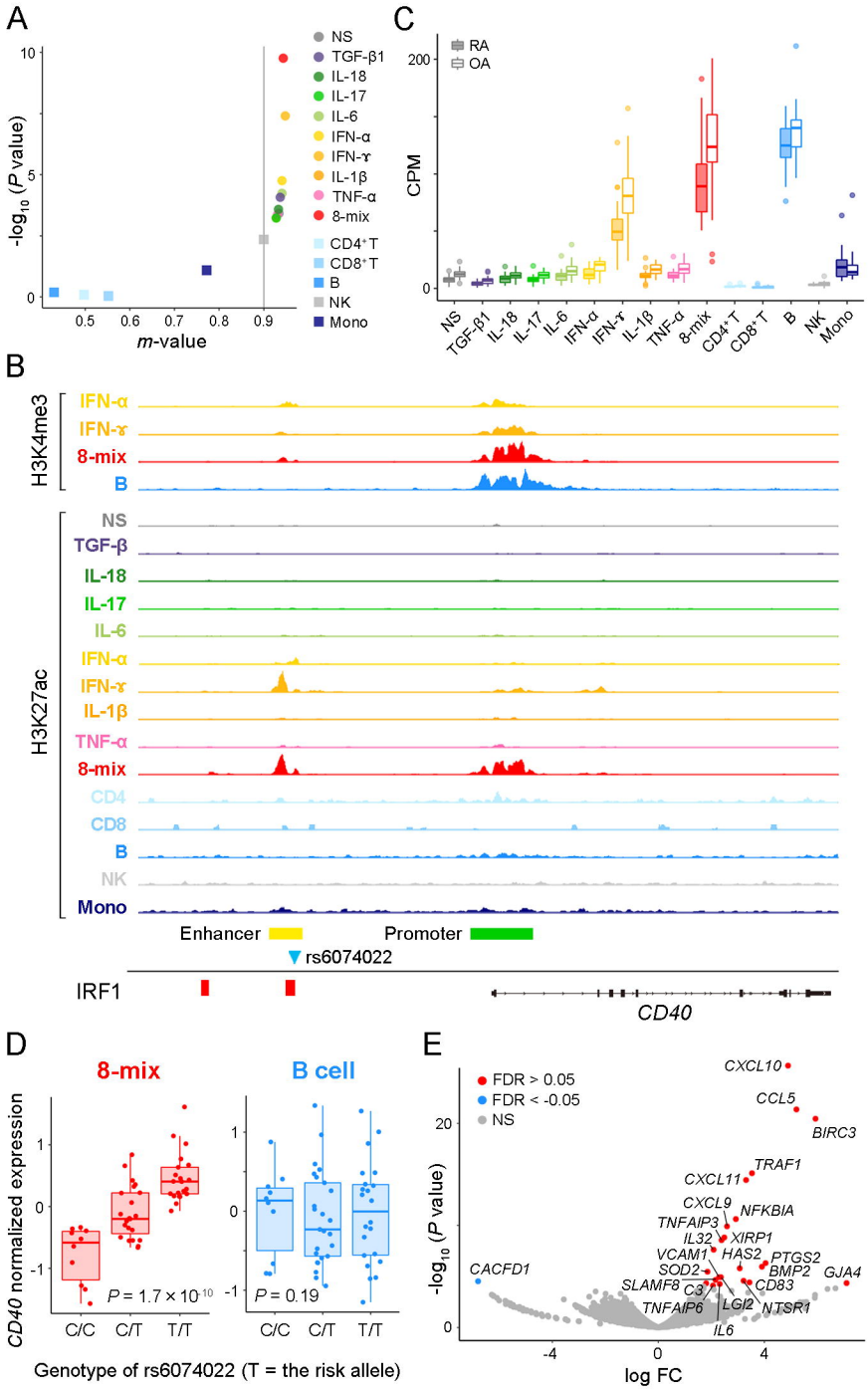

Figure 3

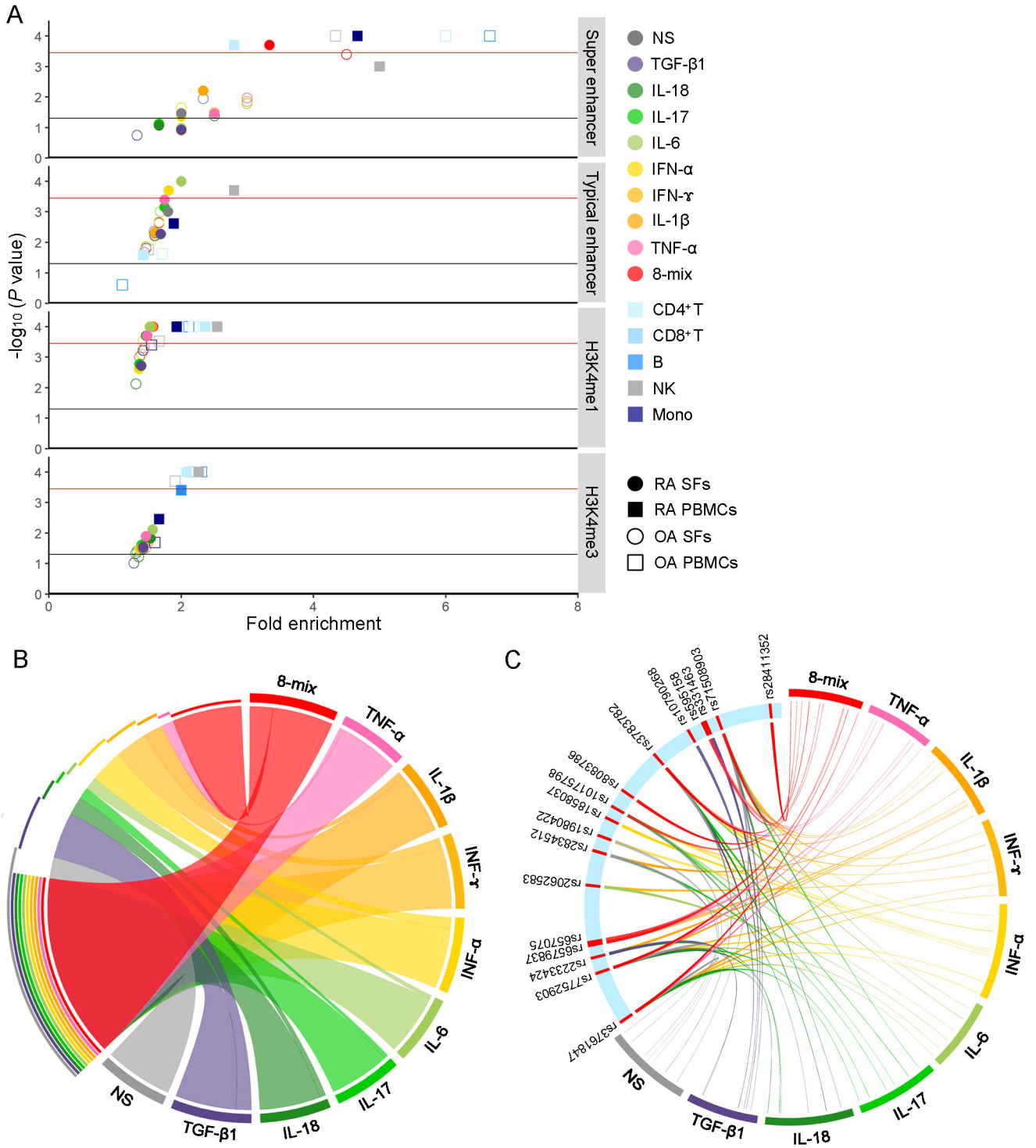

Figure 4

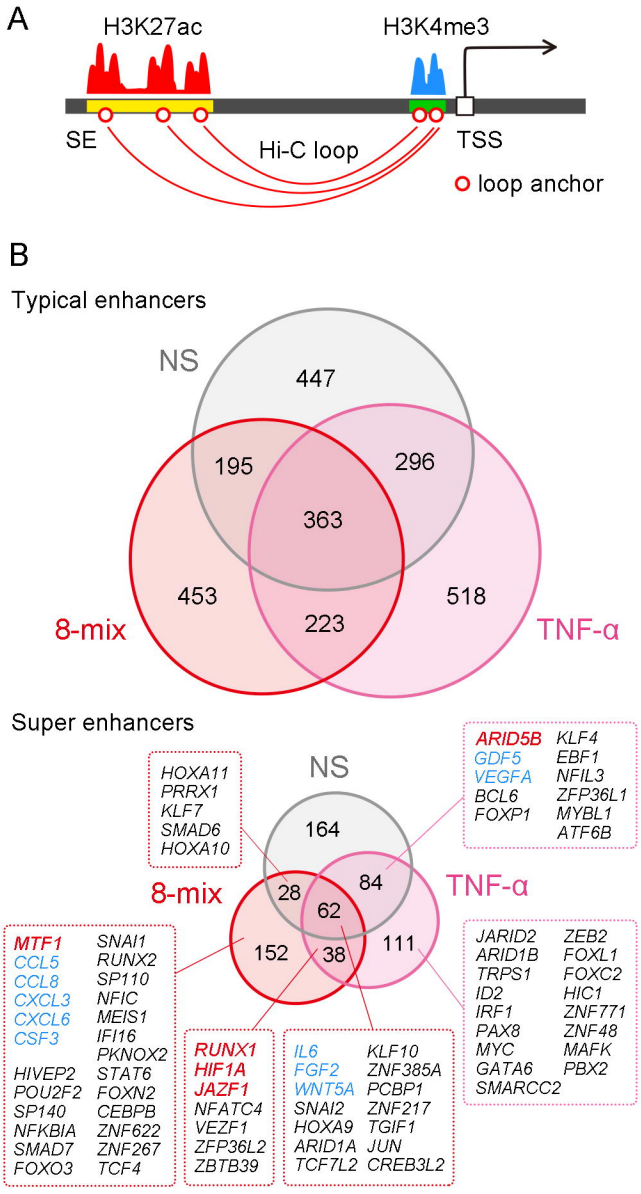

Figure 5

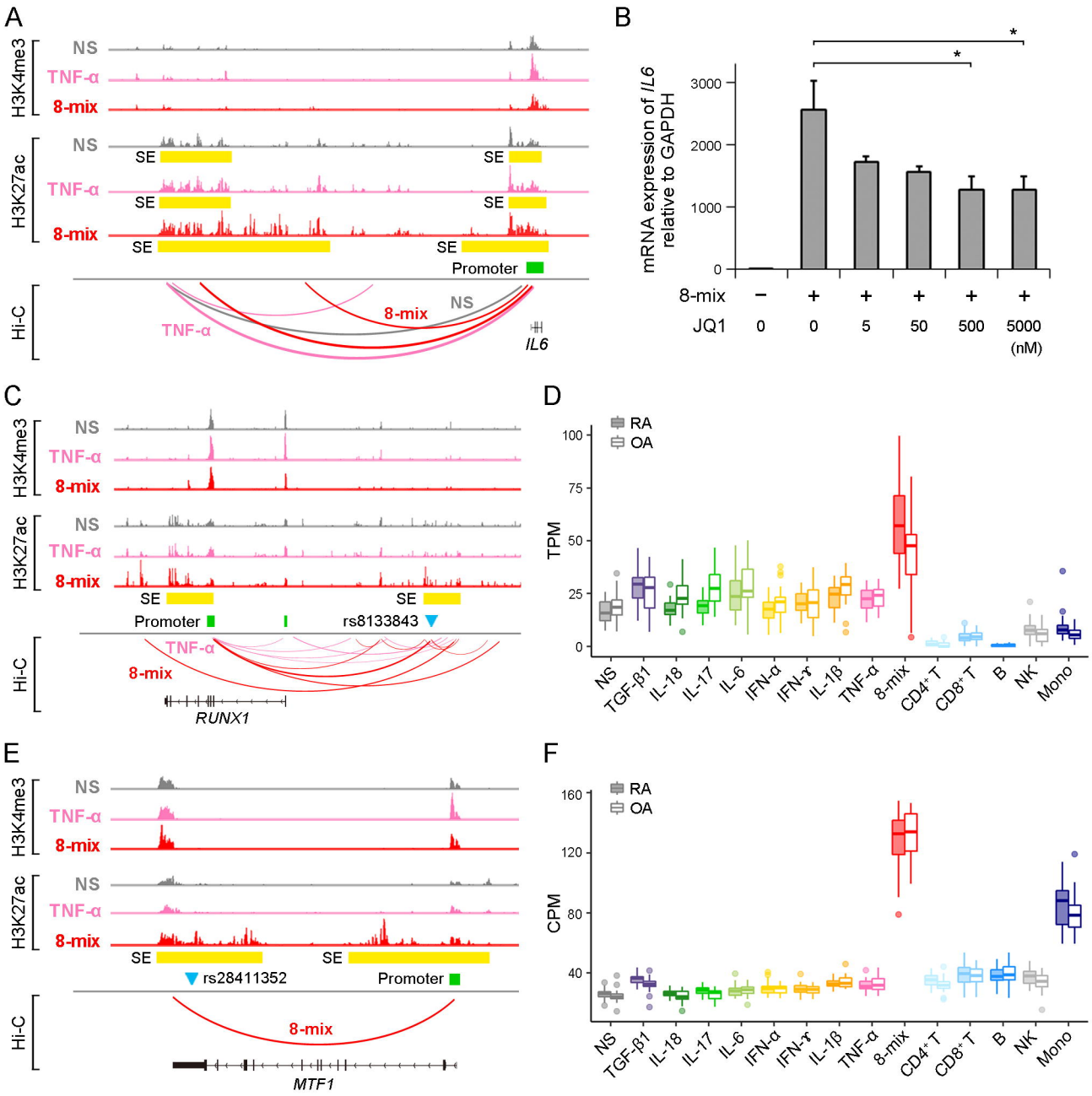

Figure 6

A

TF	Motif	SEs enrichment *P* value							
		8-mix			TNF-α			NS	
		SEs-connection	vs TEs	vs NS SEs	SEs-connection	vs TEs	vs NS SEs	SEs-connection	vs TEs
SNAI1		yes	1.0×10^{-59}	1.0×10^{-14}	no	1.0×10^{-27}	> 0.05	no	1.0×10^{-45}
TCF4		yes	1.0×10^{-50}	1.0×10^{-13}	no	1.0×10^{-22}	> 0.05	no	1.0×10^{-40}
SNAI2		yes	1.0×10^{-48}	1.0×10^{-19}	yes	1.0×10^{-22}	> 0.05	yes	1.0×10^{-34}
MTF1		yes	1.0×10^{-18}	1.0×10^{-03}	no	1.0×10^{-05}	> 0.05	no	1.0×10^{-08}
SREBF1		no	1.0×10^{-09}	1.0×10^{-09}	yes	1.0×10^{-03}	> 0.05	no	1.0×10^{-04}
RARA		no	1.0×10^{-09}	1.0×10^{-08}	no	1.0×10^{-03}	1.0×10^{-06}	yes	1.0×10^{-05}
JUN		yes	1.0×10^{-03}	1.0×10^{-14}	yes	> 0.05	> 0.05	yes	1.0×10^{-03}
FOXL1		no	1.0×10^{-08}	1.0×10^{-04}	yes	1.0×10^{-04}	> 0.05	no	1.0×10^{-05}
ZNF740		no	1.0×10^{-07}	> 0.05	no	1.0×10^{-09}	1.0×10^{-02}	yes	1.0×10^{-17}
IRF1		no	> 0.05	1.0×10^{-33}	yes	> 0.05	> 0.05	no	> 0.05
CEBPB		yes	> 0.05	1.0×10^{-30}	no	> 0.05	1.0×10^{-06}	no	> 0.05

B

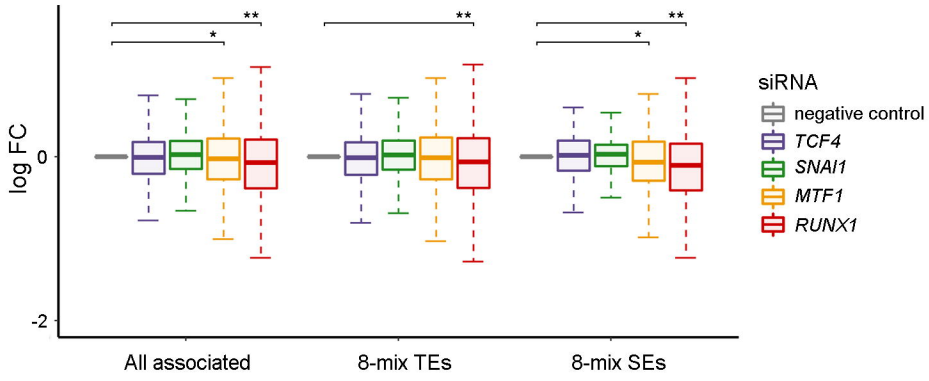

Figure 7

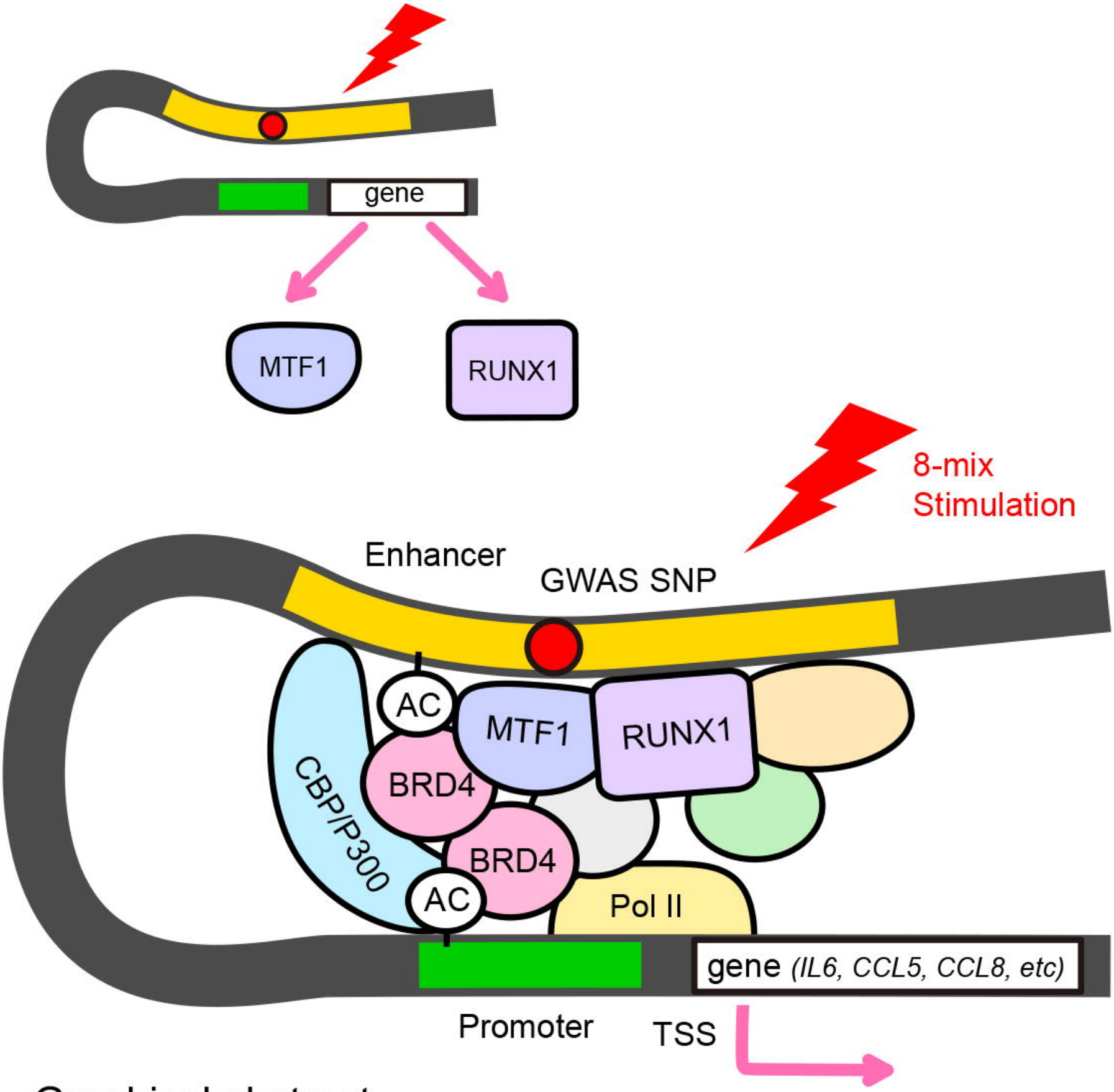

Graphical abstract